Article

Cell Stem Cell

Dedifferentiated Schwann Cell Precursors Secreting Paracrine Factors Are Required for Regeneration of the Mammalian Digit Tip

Graphical Abstract

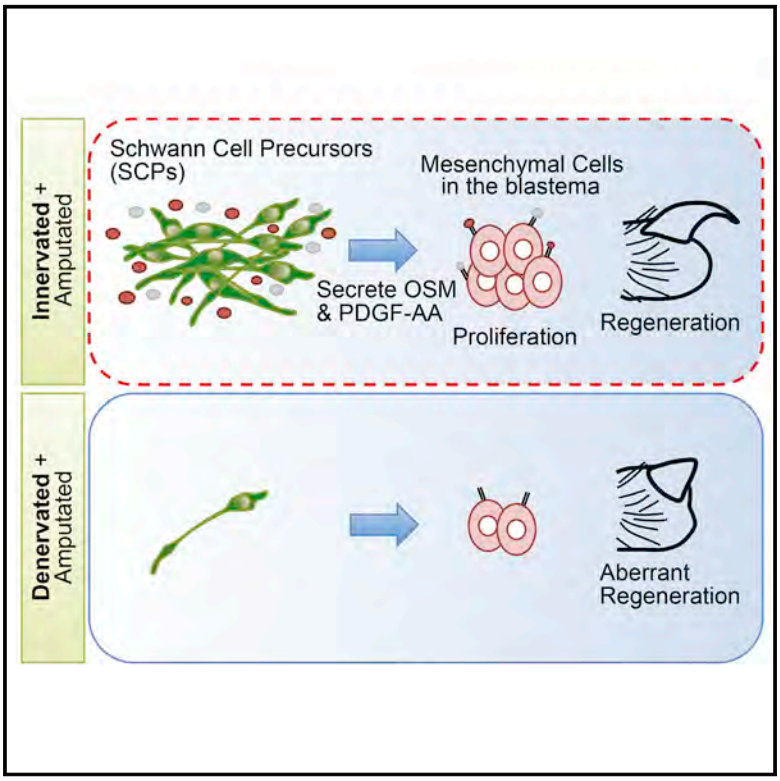

Authors

Adam P.W. Johnston, Scott A. Yuzwa, Matthew J. Carr, ..., Smitha Paul, David R. Kaplan, Freda D. Miller

Correspondence

adjohnston@upei.ca (A.P.W.J.), fredam@sickkids.ca (F.D.M.)

In Brief

Johnston et al. show that, during regeneration of the mouse digit tip, nerve-associated Schwann cell precursors dedifferentiate and move into the injured tissue, where they secrete paracrine factors, including oncostatin M and PDGF-AA, to promote mesenchymal cell proliferation, expansion of the blastema, and regeneration.

Highlights

- Schwann cell precursors (SCPs) enter the regenerating digit tip
- Ablation of SCPs by inducible deletion or denervation inhibits regeneration
- SCPs secrete growth factors to promote mesenchymal cell proliferation
- Oncostatin M and PDGF-AA can rescue regeneration in a denervated digit tip

Accession Numbers

GSE81704

Johnston et al., 2016, Cell Stem Cell *19*, 433–448
October 6, 2016
http://dx.doi.org/10.1016/j.stem.2016.06.002

Cell Stem Cell
Article

Dedifferentiated Schwann Cell Precursors Secreting Paracrine Factors Are Required for Regeneration of the Mammalian Digit Tip

Adam P.W. Johnston,[1,5,*] Scott A. Yuzwa,[1] Matthew J. Carr,[1,2] Neemat Mahmud,[1,4] Mekayla A. Storer,[1] Matthew P. Krause,[1,6] Karen Jones,[1] Smitha Paul,[1] David R. Kaplan,[1,2,3] and Freda D. Miller[1,2,3,4,7,*]
[1]Program in Neurosciences and Mental Health, Hospital for Sick Children, Toronto, ON M5G 1L7, Canada
[2]Institute of Medical Sciences
[3]Department of Molecular Genetics
[4]Department of Physiology
University of Toronto, Toronto, ON M5G 1A8, Canada
[5]Present address: Department of Applied Human Sciences, Faculty of Science, University of Prince Edward Island, Charlottetown, PE C1A 4P3, Canada
[6]Present address: Department of Kinesiology, Faculty of Human Kinetics, University of Windsor, Windsor, ON N9B 3P4, Canada
[7]Lead Contact
*Correspondence: adjohnston@upei.ca (A.P.W.J.), fredam@sickkids.ca (F.D.M.)
http://dx.doi.org/10.1016/j.stem.2016.06.002

SUMMARY

Adult mammals have lost multi-tissue regenerative capacity, except for the distal digit, which is able to regenerate via mechanisms that remain largely unknown. Here, we show that, after adult mouse distal digit removal, nerve-associated Schwann cell precursors (SCPs) dedifferentiate and secrete growth factors that promote expansion of the blastema and digit regeneration. When SCPs were dysregulated or ablated, mesenchymal precursor proliferation in the blastema was decreased and nail and bone regeneration were impaired. Transplantation of exogenous SCPs rescued these regeneration defects. We found that SCPs secrete factors that promote self-renewal of mesenchymal precursors, and we used transcriptomic and proteomic analysis to define candidate factors. Two of these, oncostatin M (OSM) and platelet-derived growth factor AA (PDGF-AA), are made by SCPs in the regenerating digit and rescued the deficits in regeneration caused by loss of SCPs. As all peripheral tissues contain nerves, these results could have broad implications for mammalian tissue repair and regeneration.

INTRODUCTION

Lower vertebrates, like amphibians, have the remarkable ability to regenerate appendages, such as limbs (Brockes and Kumar, 2002; Kragl et al., 2009; Kumar et al., 2007). However, this ability has been lost in mammals, with the exception of the distal digit. In rodents and humans, multi-tissue regeneration occurs if the digit tip is removed distal to the nail bed (Borgens, 1982; Han et al., 2008; Neufeld and Zhao, 1995). Intriguingly, there are parallels between regeneration of the murine digit tip and the amphibian limb. In both cases, there is formation of a heterogeneous blastema comprised of precursors that build the newly regenerated tissue. In amphibians, these blastema cells arise both by cellular dedifferentiation and by recruitment of tissue-resident precursor cells (Brockes and Kumar, 2002; Echeverri and Tanaka, 2002; Kragl et al., 2009). The murine digit tip blastema is also comprised of precursors of various lineages (Lehoczky et al., 2011; Rinkevich et al., 2011; Takeo et al., 2013), but it is not yet clear whether these arise by dedifferentiation or by recruitment of pre-existent precursors.

A second parallel involves nerve innervation, which is essential for normal limb regeneration in amphibians. This pro-regenerative effect is thought to be mediated by nerve-derived Schwann cells that act to promote blastema expansion (Kumar and Brockes, 2012; Kumar et al., 2007). A deficiency in mammalian digit tip regeneration also occurs following denervation (Rinkevich et al., 2014; Takeo et al., 2013; Mohammad and Neufeld, 2000), but the underlying mechanism is unclear. Intriguingly, recent research indicates that peripheral nerve innervation regulates tissue stem cell populations, including hematopoietic stem cells (Yamazaki et al., 2011; Lucas et al., 2013) and hair follicle epidermal stem cells (Brownell et al., 2011). Whereas many of these effects are thought to depend upon axonal innervation, we recently defined an important role for dedifferentiated Schwann cell precursor cells (SCPs) in skin repair (Johnston et al., 2013). In particular, skin injury caused induction of Sox2 in nerve-derived SCPs, these SCPs then moved into the regenerating dermis, and, when this process was dysregulated by inducible knockout of Sox2, skin repair was inhibited. These findings implicated SCPs in dermal repair and raised the possibility that SCPs might broadly regulate mammalian tissue repair and regeneration. Here, we have tested this idea in the context of murine digit tip regeneration and, in doing so, have defined an essential paracrine role for SCPs in adult mammalian regeneration.

RESULTS

Sox2-Positive SCPs Are Located in the Regenerating Digit Tip Blastema

We first asked whether *Sox2*-positive SCPs were present in the uninjured digit tip by examining adult mice where EGFP is knocked in to one allele of the *Sox2* gene (*Sox2*$^{EGFP/+}$ mice). *Sox2*-EGFP-positive cells were present in a pattern consistent with their localization to the innervating axon terminals (Figures 1A and S1A). All of the EGFP-positive cells also expressed S100β, a marker for Schwann cells and their precursors (Figure 1B). We asked whether these *Sox2*-positive cells were neural crest derived, using a mouse carrying a *Wnt1-Cre* transgene that is expressed in embryonic neural crest precursors and a TdTomato reporter gene with an upstream floxed stop cassette in the *Rosa26* locus (*Wnt1-Cre*;*R26-LSL-TdT* mice). We crossed these mice, where all neural crest progeny are indelibly labeled with TdTomato, to the *Sox2*$^{EGFP/+}$ mice. Analysis of distal digit sections showed that virtually all *Sox2*-EGFP-positive cells were also positive for TdTomato (Figure 1C).

We also examined mice carrying a tamoxifen-inducible CreERT2 knocked in to the *Sox2* gene and the same TdTomato reporter gene (*Sox2*$^{CreERT2/+}$; *R26-LSL-TdT* mice). Following tamoxifen administration, *Sox2CreERT2*-TdTomato-positive cells were observed to be associated with terminal axons throughout the distal digit (Figure 1D), and these all expressed the p75 neurotrophin receptor (p75NTR), which marks SCPs, peripheral axons, and S100β (Figures 1E and 1F). These neural crest-derived, Sox2-positive SCPs are likely analogous to the nerve terminal (NT) cells we previously characterized in hair follicles (Johnston et al., 2013).

We next examined digit tip regeneration by removing the digit distal to the nail bed in adult mice. In this model, by 2 weeks, bone and nail regeneration has commenced, and by 4 weeks, regeneration is largely complete (Figures S1B and S1C). We first performed these experiments in mice expressing EGFP from the *PDGFRα* gene (*PDGFRα*$^{EGFP/+}$ mice), because platelet-derived growth factor receptor α (PDGFRα) marks diverse mesenchymal precursors (Farahani and Xaymardan, 2015) and allowed us to visualize the blastema. Immunostaining 1 week post-amputation identified a small blastema containing many *PDGFRα*-EGFP-positive mesenchymal cells and CD31-positive blood vessels (Figure 1G). Immunostaining for the epidermal marker keratin 14 (K14) showed that the wound epithelium had already reformed over the tip of the injured digit (Figure 1H). By 2 and 3 weeks, regeneration was apparent, and the distal blastema still included many *PDGFRα*-EGFP-positive mesenchymal cells and CD31-positive blood vessels (Figures 1G and 1H). By 4 weeks, digit tip regeneration was largely complete (Figures 1G, 1H, S1B, and S1C).

To ask about the location of SCPs during regeneration, we removed the distal digits in *Sox2*$^{CreERT2/+}$; *R26-LSL-TdT* mice and treated them with tamoxifen for 4 days starting at the time of injury. Two weeks later, many *Sox2CreERT2*-TdTomato-positive cells were present within the regenerating tissue and the adjacent large nerve bundles (Figure 1I). These cells were positive for S100β and p75NTR but were not associated with axons expressing the general axonal marker PGP9.5 (Figures 1J–1L). In contrast, PGP9.5-positive axons and *Sox2*-positive SCPs were closely associated in the adjacent, uninjured tissue (Figure 1L). By 4 weeks post-amputation, TdTomato-positive, S100β-positive SCPs were again associated with PGP9.5-positive axons and were distributed in a pattern reminiscent of the uninjured digit (Figures 1M–1O), although they were more disorganized (compare Figure 1M to 1D). We confirmed that these SCPs were neural crest derived by examining *Sox2*$^{EGFP/+}$;*Wnt1-Cre*;*R26-LSL-TdT* mice. At 2 weeks post-amputation, virtually all *Sox2*-EGFP-positive cells were also TdTomato positive (Figure 1P).

We performed similar experiments in regenerating digit tips of *PDGFRα*$^{EGFP/+}$ mice. From 1 to 3 weeks post-amputation, S100β-positive SCPs were present in the regenerated tissue and in the blastema, where they were mingled with *PDGFRα*-EGFP-positive and negative cells (Figures 2A and S2A). By 4 weeks, the pattern of S100β-positive SCPs was similar to that seen in the *Sox2*$^{CreERT2/+}$; *R26-LSL-TdT*$^{+}$ mice (compare the 28-DPA image in Figure 2A to Figures 1M–1O).

We next characterized axons over this time course (Figure S2B). At 1 and 2 weeks post-amputation, virtually no PGP9.5-positive axons were present in the blastema, although at 2 weeks, a few were present in the adjacent regenerated tissue. By 3 weeks, axons were more abundant at the periphery of the blastema, and at 4 weeks, axons were present throughout the regenerated digit tips (Figure S2B). Similar results were obtained examining *Sox2*$^{EGFP/+}$ mice. At 1 and 2 weeks post-amputation, *Sox2*-EGFP-positive SCPs were present in the blastema, but very few of these were colocalized with PGP9.5-positive axons (Figure S2C). Thus, for 2 to 3 weeks post-amputation, SCPs, but not axons, are present in the regenerating blastema (Figure S2D).

Denervation Prevents SCPs from Entering the Regenerating Tissue and Inhibits Digit Tip Regeneration

On the basis of these findings, we asked whether denervation reduces digit tip regeneration by inhibiting the SCP injury response. Specifically, we resected the sciatic nerve in *Sox2*$^{CreERT2/+}$;*R26-LSL-TdT* mice and waited 10 days to allow complete distal axon degeneration. This type of nerve injury permanently inhibits axonal regeneration. We then removed the digit tip and administered tamoxifen for 4 days. Analysis 4 weeks later showed that *Sox2CreERT2*-TdTomato-positive, S100β-positive SCPs were absent from the denervated, regenerated digit tips, although they were present in innervated, regenerated controls (Figures 2B and 2C). To better characterize this denervation-induced loss of SCPs, we examined *Sox2*$^{EGFP/+}$ mice. At 5 and 10 days following sciatic nerve resection (prior to amputation), all axons were gone from the denervated digit tips, but *Sox2*-EGFP-positive, S100β-positive SCPs were still present (Figures 2D and 2E). However, at 1 or 2 weeks following amputation, there were virtually no *Sox2*-EGFP-positive SCPs in the blastema or newly regenerated tissue, although scattered positive cells were present in the adjacent, uninjured tissue (Figures 2F and S2E). In contrast, CD31-positive blood vessels and K14-positive epithelial cells were apparently similar between denervated and control regenerating digits (Figures 2G and S2F).

To ask whether this loss of SCPs had any effect, we unilaterally resected the sciatic nerve, removed the digit tip 10 days later, and characterized regeneration. As an internal control,

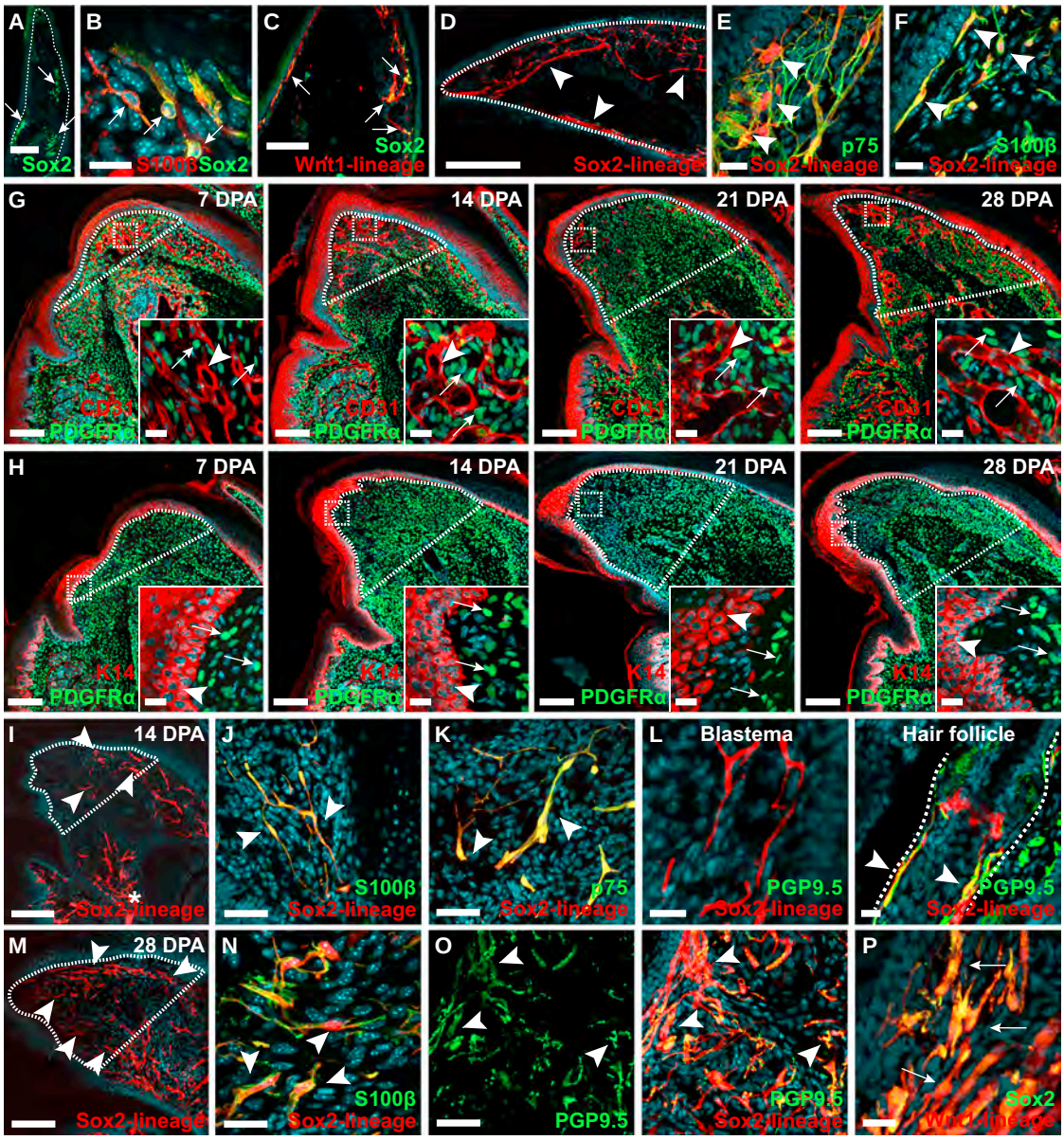

Figure 1. Sox2-Positive SCPs in Intact and Regenerating Adult Murine Distal Digits

(A and B) Confocal images of uninjured distal digits from adult *Sox2*$^{EGFP/+}$ mice immunostained for EGFP (Sox2, green) and S100β (red, B). Arrows denote single- (A) or double-positive (B) cells.

(C) Confocal images of the distal digit of a *Sox2*$^{EGFP/+}$; *Wnt1-Cre*;*R26-LSL-TdT* mouse immunostained for *Sox2*-EGFP (green) and TdTomato (red, Wnt1-lineage). Arrows denote double-positive cells.

(D–F) Confocal images of distal digits of uninjured *Sox2*$^{CreERT2/+}$; *R26-LSL-TdT* mice tamoxifen treated for 4 days, immunostained for TdTomato (Sox2-lineage, red) and p75NTR (E, green) or S100β (F, green). Arrowheads denote single- (D) or double-labeled (E and F) cells.

(G and H) Confocal images of distal digits of *PDGFRα*$^{EGFP/+}$ mice at 7, 14, 21, and 28 days post-amputation (DPA), immunostained for *PDGFRα*-EGFP (PDGFRα, green), and CD31 (red, G) or K14 (red, H). Boxed regions in the blastema are shown at higher magnification in the insets. Arrowheads in (G) and (H) denote CD31-positive blood vessels and K14-positive epithelium, respectively, and arrows *PDGFRα*-EGFP-positive cells.

(I–O) Confocal images of digits of *Sox2*$^{CreERT2/+}$;*R26-LSL-TdT* mice that were amputated, tamoxifen treated, and immunostained 14 (I–L) or 28 (M–O) DPA for TdTomato (Sox2-lineage, red) and S100β (green, J and N), p75NTR (K, green), or PGP9.5 (green, L and O). The left and right images in (L) are the blastema and a hair follicle in the adjacent uninjured tissue, respectively. Arrowheads in (I) and (M) denote single-labeled cells, in (J), (K), and (N), double-labeled cells and, in (L) and (O), TdTomato-positive cells associated with PGP9.5-positive axons. The asterisk in (I) indicates a TdTomato-positive nerve bundle.

(P) Confocal image of the 2-week regenerating digit of a *Sox2*$^{EGFP/+}$;*Wnt1-Cre*;*R26-LSL-TdT* mouse, immunostained for *Sox2*-EGFP (Sox2, green) and TdTomato (Wnt1-lineage, red). Arrows denote double-labeled cells. All panels except (A) and (O) (left image) were counterstained with Hoechst 33258 (blue). In (G)–(I) and (M), hatched white lines outline the regenerating tissue exclusive of the epithelium and, in (A) and (D), the uninjured digit. The scale bars in (A), (C), (D), (G)–(I), and (M) represent 200 μm and (J), (K), and (O) represent 50 μm; (B), (E), (F), (G, insets), (H, insets), (L), and (N), p = 20 μm.

See also Figure S1.

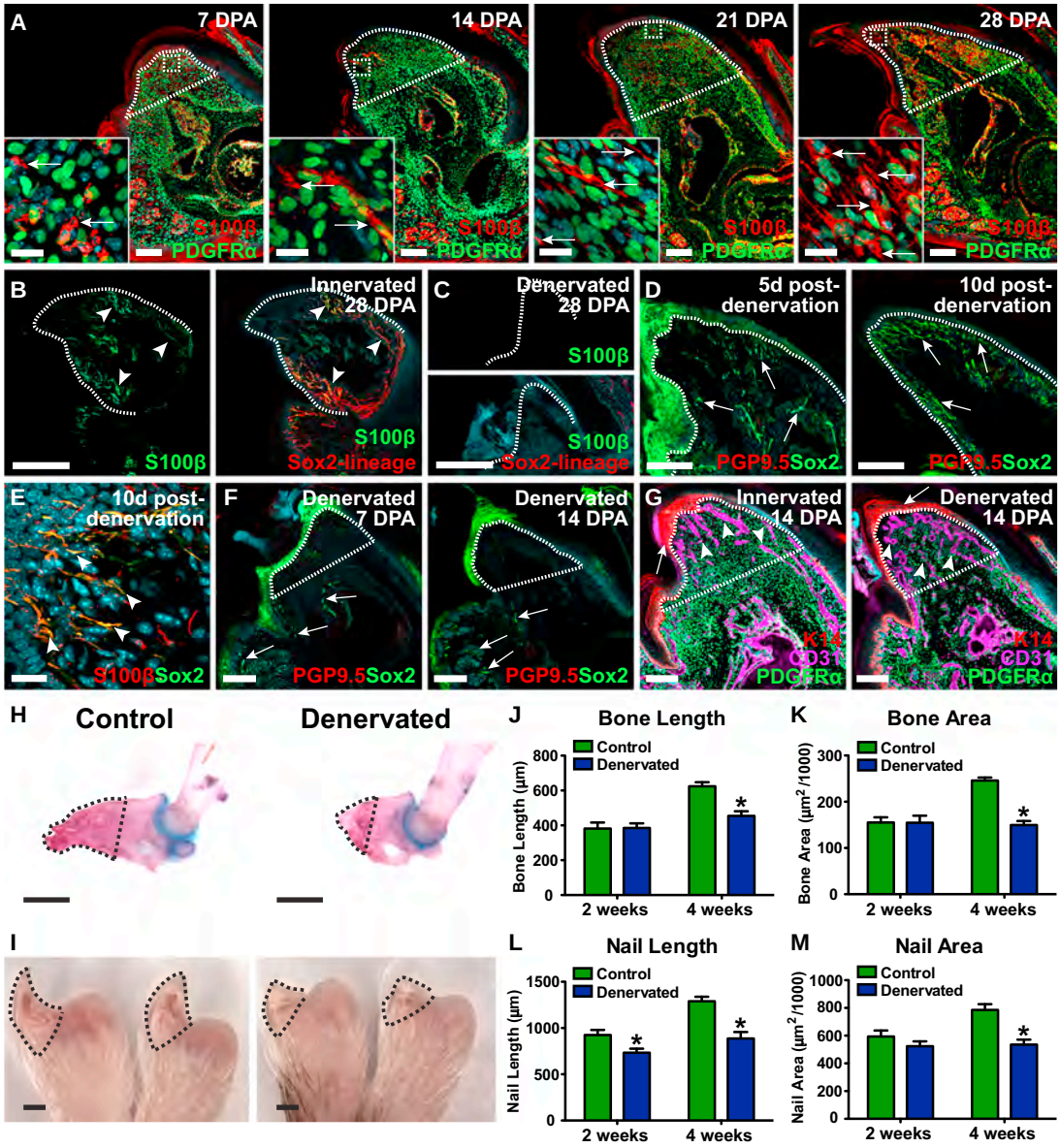

Figure 2. Denervation Prevents the Appearance of Sox2-Positive SCPs in the Regenerating Digit Tip and Impairs Regeneration

(A) Confocal images of distal digits of *PDGFRα*$^{EGFP/+}$ mice 7, 14, 21, and 28 DPA, immunostained for *PDGFRα*-EGFP (PDGFRα, green) and S100β (red). The boxed regions in the blastema are shown at higher magnification in the insets. Arrows indicate S100β-positive SCPs.

(B and C) Images of distal digits of *Sox2*$^{CreERT2/+}$;*R26-LSL-TdT* mice that were (C) or were not (B) denervated and then were amputated and tamoxifen treated, at 28 DPA, immunostained for TdTomato (Sox2-lineage, red) and S100β (green). Arrowheads denote double-labeled cells.

(D and E) Confocal images of uninjured distal digits of *Sox2*$^{EGFP/+}$ mice that were denervated by sciatic nerve resection 5 days (5d; left panel, D) or 10 days (10d; right panel, D and E) earlier, immunostained for EGFP (Sox2, green) and PGP9.5 (red, D) or S100β (red, E). Arrows in (D) denote *Sox2*-EGFP-positive cells (green epithelial staining is background), and arrowheads in (E) denote double-labeled SCPs.

(F) Confocal images of denervated, distal digits of *Sox2*$^{EGFP/+}$ mice 7 (left panel) and 14 (right panel) DPA, immunostained for EGFP (Sox2, green) and PGP9.5 (red). Arrows indicate *Sox2*-EGFP-positive cells in adjacent uninjured tissue (green epithelial staining is background).

(G) Confocal images of distal digits of *PDGFRα*$^{EGFP/+}$ mice 14 DPA that were or were not denervated, immunostained for *PDGFRα*-EGFP (PDGFRα, green), CD31 (purple), and K14 (red). Arrows and arrowheads denote K14-positive epithelium and CD31-positive blood vessels, respectively.

(H–M) The sciatic nerve of adult mice was unilaterally resected, 10 days later digit tips were amputated, and regeneration was characterized 2 or 4 weeks post-amputation. (H and I) Representative images of the distal bones (H) or nails (I) of regenerated digits from a denervated foot or a contralateral normally innervated foot (control) 4 weeks post-amputation are shown. Bones in (H) were stained with Alizarin red and Alcian blue, and nails (I) were imaged as whole mounts. Black hatched lines outline the regenerated tissue. (J–M) The extent of regeneration was quantified by measuring the length and area of the regenerated bone (J and K) and nail (L and M) from images as in (H) and (I). *$p < 0.05$; $n = 8$ digits per group.

In (A)–(G), sections were counterstained with Hoechst 33258 (blue). In (A)–(C), (F), and (G), hatched white lines outline the regenerating tissue exclusive of the epithelium and, in (D), the uninjured digit. Error bars denote SEM. The scale bars in (A), (B), (C), (D), (F), and (G) represent 200 μm; (A) (insets) and (E) represent 20 μm; and (H) and (I) represent 500 μm. See also Figure S2.

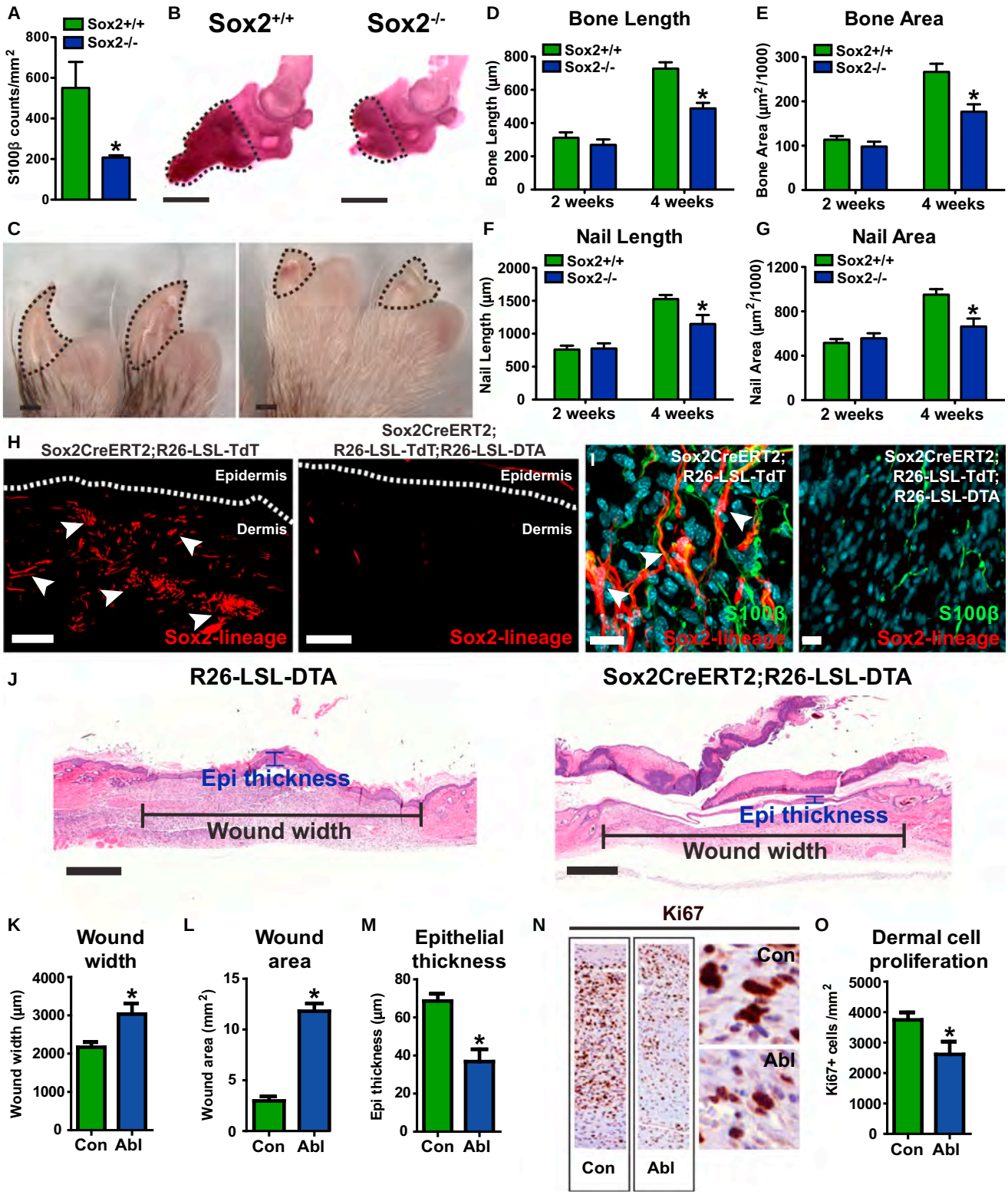

Figure 3. Inducible Deletion of Sox2 Inhibits Digit Tip Regeneration, and Inducible Ablation of Sox2-Positive SCPs Impairs Skin Repair

(A–G) Adult *Sox2*$^{fl/fl}$;*R26-CreERT2* mice (Sox2$^{-/-}$) were treated with tamoxifen for 5 days, distal digit tips were amputated 1 week later, and regeneration was characterized 2 or 4 weeks post-amputation. As a control, *Sox2*$^{fl/fl}$ mice that did not carry CreERT2 (Sox2$^{+/+}$) were treated similarly. (A) Quantification of the density of S100β-positive SCPs in the regenerating digit tip tissue 2 weeks post-amputation is shown. *$p < 0.05$, n = 3–4 mice per group, one digit each, three sections per digit. (B and C) Representative images of the distal bones (B) or nails (C) of regenerated digits 4 weeks post-amputation are shown. Bones in (B) were

(legend continued on next page)

we amputated digits from the contralateral, normally innervated paws of the same animals. Analysis 4 weeks later showed that denervation inhibited regeneration of the bone and nail of the injured digits (Figures 2H and 2I). Quantification showed that denervation had no effect on the length or area of the regenerated bones at 2 weeks but that, by 4 weeks, both were significantly decreased (Figures 2J and 2K). As for nail regeneration, nail length, but not area, was already modestly decreased by denervation at 2 weeks, and by 4 weeks, both of these measures were significantly decreased (Figures 2L and 2M). Thus, prior denervation inhibits digit tip regeneration coincident with a loss of SCPs from the regenerating tissue.

Inducible Knockout of Sox2 Inhibits Digit Tip Regeneration

As a second experiment to ask whether SCPs were involved in digit tip regeneration, we acutely knocked out Sox2, using *Sox2*$^{fl/fl}$ mice carrying a ubiquitously expressed CreERT2 gene (*Sox2*$^{fl/fl}$;*R26-CreERT2* mice). We treated these mice with tamoxifen for 5 days, a treatment that causes almost complete genetic ablation of Sox2 (Johnston et al., 2013), and removed their distal digits 1 week later. As controls, we performed similar experiments with *Sox2*$^{fl/fl}$ mice lacking CreERT2. Immunostaining for S100β 2 weeks later demonstrated that the density of SCPs in the regenerating digit tip was significantly decreased by acute deletion of *Sox2* (Figure 3A). We then characterized bone and nail regeneration (Figures 3B–3G). As seen with denervation, at 2 weeks, nail and bone regeneration was similar to controls, but by 4 weeks, the length and area of the regenerated bone and nail were significantly decreased relative to controls. Thus, Sox2 is essential for normal digit tip regeneration, likely through its actions in SCPs.

Inducible Ablation of SCPs Inhibits Skin Repair and Digit Tip Regeneration

We used one final approach to ask about SCPs and regeneration, using mice carrying an active diphtheria toxin A (DTA) fragment with an upstream floxed stop cassette in the *Rosa26* locus (*R26-LSL-DTA* mice) crossed to *Sox2*$^{CreERT2/+}$ mice and, in some experiments, to *R26-LSL-TdT* mice to enable us to visualize targeted cells. In these mice, tamoxifen treatment causes expression of DTA and TdTomato in *Sox2*-positive cells, leading to death of SCPs.

We confirmed that this strategy worked using a skin repair paradigm. We performed full thickness punch wounds on back skin of *Sox2*$^{CreERT2/+}$;*R26-LSL-DTA*;*R26-LSL-TdT* mice, treated them with tamoxifen for 4 days, and analyzed TdTomato expression 5 days later (9 days post-injury; Figures 3H and 3I). In control *Sox2*$^{CreERT2/+}$;*R26-LSL-TdT* mice, there were many *Sox2CreERT2*-TdTomato-positive, S100β-positive SCPs within the regenerating dermis, but virtually none were seen in the dermis of mice carrying the *R26-LSL-DTA* allele. However, a few S100β-positive, TdTomato-negative cells were still observed, presumably because they were Schwann cells that did not express *Sox2* and/or because *Sox2*-CreERT2 was not fully penetrant.

We then asked whether this manipulation affected skin repair, analyzing skin sections from *Sox2*$^{CreERT2/+}$;*R26-LSL-DTA* versus control *R26-LSL-DTA* mice 9 days post-injury. Morphometric analysis (Johnston et al., 2013; Naska et al., 2016) showed that depletion of SCPs caused a significant deficit in skin wound healing (Figure 3J). Relative to controls, wound width and area were significantly increased and epithelial thickness was significantly decreased (Figures 3K–3M). Moreover, dermal cells expressing the proliferation marker Ki67 were significantly decreased (Figures 3N and 3O).

We used the same strategy to ask about digit tip regeneration, removing digit tips from the same groups of mice and treating them with tamoxifen for 4 days. Analysis 2 weeks later showed that *Sox2CreERT2*-TdTomato-positive, S100β-positive SCPs were decreased in regenerating digits of mice carrying the *R26-LSL-DTA* allele (Figure 4A). In contrast, CD31-positive blood vessels and K14-positive epithelial cells were apparently similar in both groups of mice at this time point (Figure 4B). We then characterized bone and nail regeneration (Figures 4C–4H). At 2 weeks, DTA-mediated ablation of SCPs caused a significant decrease in nail regeneration, although there was no difference in bone regeneration. However, by 4 weeks, all measures of bone and nail regeneration were significantly decreased by SCP ablation (Figures 4C–4H). Thus, when SCPs were inducibly ablated at the time of injury, this impaired both skin repair and digit tip regeneration.

Transplantation of SCPs Rescues the Denervation-Induced Deficits in Digit Tip Regeneration

One prediction of these findings is that transplantation of exogenous SCPs in the absence of axons might rescue the denervation-induced digit tip regeneration deficits. We tested this prediction, using SCPs isolated from the neonatal rat sciatic nerve and expanded in culture (Krause et al., 2014). We

stained with Alizarin red and Alcian blue, and nails (C) were imaged as whole mounts. Black hatched lines outline the regenerated bones and nails. (D–G) The extent of regeneration was quantified by measuring the length and area of the regenerated bone (D and E) and nail (F and G) from images as in (B) and (C). *$p < 0.05$; n = 8–14 digits per group.

(H and I) *Sox2*$^{CreERT2/+}$;*R26-LSL-TdT*;*R26-LSL-DTA* and control *Sox2*$^{CreERT2/+}$;*R26-LSL-TdT* mice received 6-mm-diameter full thickness punch wounds to the dorsal skin, were tamoxifen treated, and analyzed 9 days post-injury. Shown are confocal images of regenerated skin immunostained for TdTomato (Sox2-lineage, red) and S100β (I, green) and counterstained with Hoechst 33258 (I, blue). Hatched white lines (H) denote the border between the dermis and epidermis, and arrowheads indicate single (H) and double-labeled (I) SCPs.

(J–O) *Sox2*$^{CreERT2/+}$;*R26-LSL-DTA* (Abl) and control *R26-LSL-DTA* (Con) mice received 6-mm-diameter full thickness punch wounds to the dorsal skin, were tamoxifen treated, and analyzed 9 days post-injury. (J) Representative images of H&E-stained paraffin sections of regenerating skin 9 days post-injury are shown. Black bars indicate wound width and blue bars epidermal (Epi) thickness. (K–M) Images as in (J) were quantified for wound width (K), wound area (L), and epidermal thickness (M). *$p < 0.05$; n = 10–13 per group. (N and O) Representative images (N) of paraffin sections of regenerating skin immunostained for Ki67 (N, brown; counterstained with hematoxylin in purple) and quantified for the density of Ki67-positive cells within the regenerating dermis (O) are shown. *$p < 0.05$; n = 10–13 per group.

Error bars denote SEM. The scale bars in (B), (C), and (J) represent 500 μm; (H) represents 200 μm; and (I) represents 20 μm.

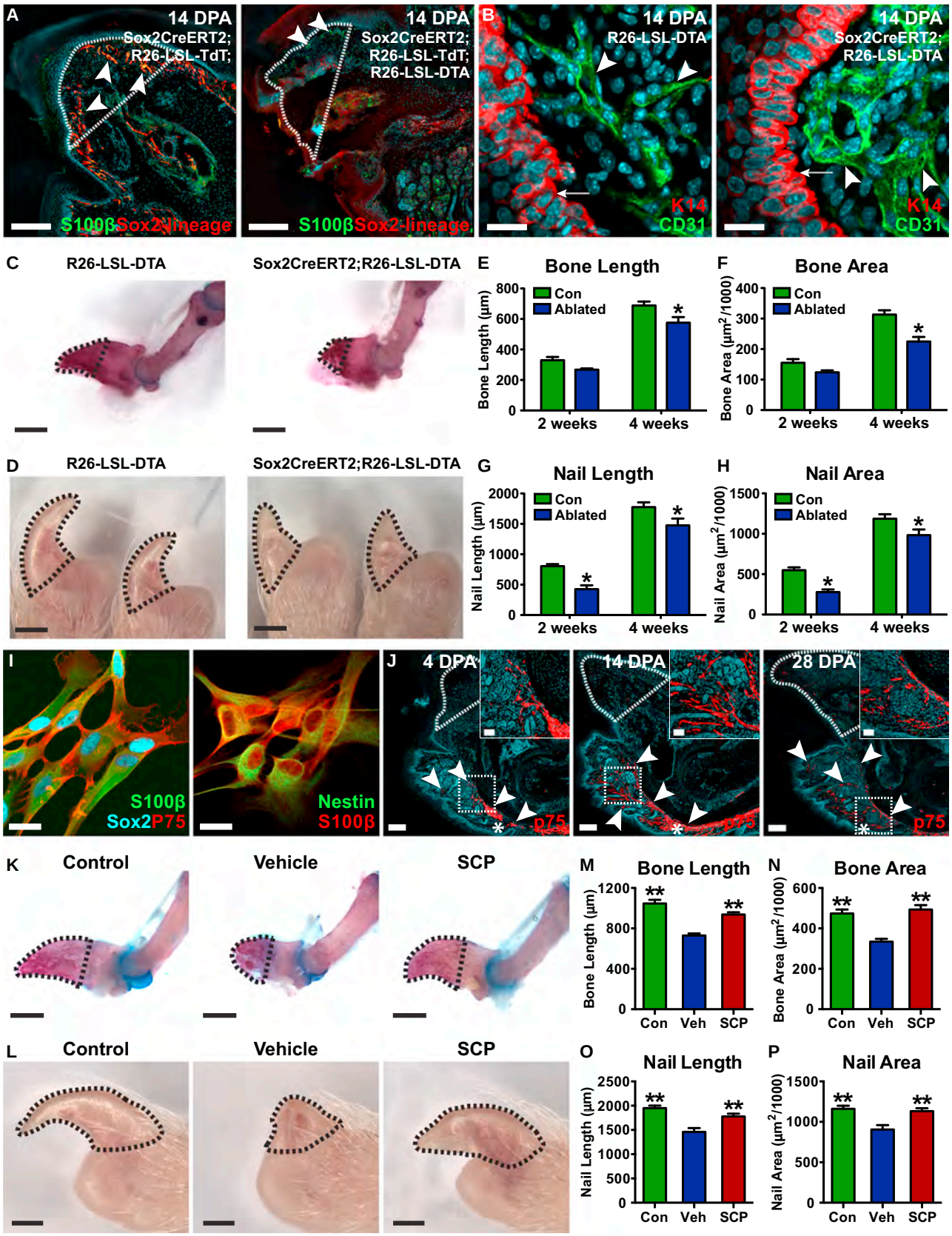

(legend on next page)

confirmed that, like SCPs in vivo, these cultured SCPs expressed Sox2, nestin, S100β, and p75NTR (Figure 4I). We then denervated immunocompromised adult non-obese diabetic (NOD)-severe combined immunodeficiency (SCID) mice by sciatic nerve resection, removed their distal digits 10 days later, and, after a further 3 days, transplanted SCPs immediately proximal to the digit injury. As controls, we injected the transplant vehicle alone. Immunostaining with a rat-specific p75NTR antibody showed that many rat SCPs were present close to the injection site at 4 days post-amputation and that, by 2 and 4 weeks, these transplanted cells were more broadly distributed adjacent to the regenerating tissue (Figure 4J). Immunostaining for PGP9.5 confirmed the complete absence of axons in transplanted digits at 2 and 4 weeks post-amputation (Figure S3A).

We then characterized regeneration following SCP transplantation (Figures 4K–4P, S3B, and S3C). At 4 weeks, denervated digits injected with vehicle alone did not regenerate well, but denervated digits transplanted with SCPs regenerated almost as well as normally innervated, regenerated digits. However, in some SCP-transplanted digits, the morphologies of the regenerated nail and bone were somewhat aberrant, suggesting that location of SCPs relative to the blastema is important for patterning.

SCPs Secrete Growth Factors to Promote Mesenchymal Precursor Self-Renewal

One explanation for these findings is that SCPs secrete growth factors to promote blastema expansion and thus regeneration. To test this idea, we unilaterally denervated adult *PDGFRα*$^{EGFP/+}$ mice, amputated their digit tips 10 days later, administered EdU at 13 days post-amputation, and analyzed ipsilateral, denervated and contralateral, innervated digits 1 day later. For both groups of digits, EdU-positive cells were particularly abundant within the distal blastema tissue and in the nail bed epithelium (Figure 5A). Most of the EdU-positive blastema cells were *PDGFRα*-EGFP positive, although some EdU-positive, EGFP-negative cells were associated with blood vessels, likely endothelial cells (Figure 5B). However, the percentage of *PDGFRα*-EGFP-positive cells that were also positive for EdU and the density of EdU-positive cells were both significantly decreased in the denervated digits (Figures 5C, 5D, S4A, and S4B).

To define candidate growth factors for this potential SCP proliferative activity, we asked whether SCPs secreted factors that enhanced self-renewal of skin-derived precursors (SKPs), dermal mesenchymal precursors that can reconstitute the dermis and may be relevant for digit tip regeneration (Toma et al., 2001; Biernaskie et al., 2009). Specifically, we plated purified neonatal rat sciatic nerve SCPs in medium containing neuregulin but no serum, collected this conditioned medium after 5–7 days, and added it to dissociated secondary passage neonatal rat SKPs. As a negative control, we used unconditioned SCP medium, and as a positive control, we used optimal SKPs growth medium containing FGF2 and EGF. Analysis 1 week later showed that SCP-conditioned medium significantly increased the number and size of SKP spheres and that it was as potent as optimal SKPs growth medium in doing so (Figures 5E and 5F). We confirmed this proliferative effect by immunostaining SKP cultures for Ki67 (Figure 5G).

To identify the SCP growth factors that mediated these effects, we defined potential ligand-receptor interactions by transcriptome analysis. For ligands, we extracted RNA from three independent biological replicates of cultured neonatal rat sciatic nerve SCPs, analyzed them on Rat Gene 2.0 ST arrays (Table S1; GEO: GSE81704), and extracted potential ligands from a curated growth factor database (Qiao et al., 2014). We considered any ligand mRNAs that had expression values of at least 50% of the highest $\log_2$ expression values in the dataset (Kirouac et al., 2010). This analysis identified 74 potential SCP-secreted ligands (Table S2). We performed a similar transcriptome analysis (Table S1; GEO: GSE81704) to identify growth factor receptors expressed by adult rat dorsal dermis SKPs, using the same

Figure 4. Inducible Ablation of SCPs Inhibits Digit Tip Regeneration, and the Denervation-Induced Regeneration Deficits Can Be Rescued by Transplantation of Exogenous SCPs

(A) Representative images of distal digits of *Sox2*$^{CreERT2/+}$;*R26-LSL-TdT*;*R26-LSL-DTA* and control *Sox2*$^{CreERT2/+}$;*R26-LSL-TdT* mice that were amputated, tamoxifen treated, and immunostained 14 DPA for TdTomato (Sox2-lineage, red) and S100β (green). Arrowheads denote double-labeled (left) and S100β-positive (right) cells.

(B) Confocal images of digit tips from control *R26-LSL-DTA* mouse and *Sox2*$^{CreERT2/+}$;*R26-LSL-DTA* mice treated with tamoxifen and immunostained 14 DPA for K14 (red) and CD31 (green). Arrows and arrowheads denote K14-positive epithelium and CD31-positive blood vessels.

(C–H) Adult *Sox2*$^{CreERT2/+}$;*R26-LSL-DTA* (ablated) and control *R26-LSL-DTA* (con) mice had digit tips amputated, were tamoxifen treated, and analyzed for regeneration 2 and 4 weeks post-amputation. (C and D) Representative images of the bone (C) or nail (D) of regenerated digit tips 4 weeks post-amputation are shown. Bones in (C) were stained with Alizarin red and Alcian blue, and nails (D) were imaged as whole mounts. Black hatched lines outline the regenerated tissues. (E–H) The extent of regeneration was quantified by measuring the length and area of the bone (E and F) and nail (G and H) from images as in (C) and (D). *$p < 0.05$; n = 8–18 digits per group.

(I) Images of cultured neonatal rat SCPs immunostained for (left panel) Sox2 (blue), p75 neurotrophin receptor (red), and S100β (green) or for (right panel) nestin (green) and S100β (red).

(J–P) Adult NOD-SCID mice were denervated, 10 days later ipsilateral digit tips were amputated, and 3 days later 500,000 rat SCPs (as in I) were transplanted into the digit pad proximal to the amputation plane. As controls, mice were not denervated (con) or were transplanted with vehicle alone (veh). (J) Confocal images of transplanted digit tips at 4, 14, and 28 DPA, immunostained with a rat-specific p75NTR antibody (red) to detect transplanted cells, are shown. The boxed regions are close to the transplant sites (indicated with asterisks) and are shown at higher magnification in top right corner insets. Arrowheads denote transplanted cells. (K and L) Representative images of the bone (K) or nail (L) of regenerated digit tips 4 weeks post-amputation. Bones in (K) were stained with Alizarin red and Alcian blue, and nails (L) were imaged as whole mounts. Black hatched lines outline the regenerated tissues. (M–P) The extent of regeneration was quantified by measuring the length and area of the bone (M and N) and nail (O and P) from images as in (K) and (L). **$p < 0.01$ by one-way ANOVA with Dunnett's post hoc analysis; n = 21 digits for the control group and 8–12 digits per experimental group.

In (A), (B), and (J), sections were counterstained with Hoechst 33258 (blue). In (A) and (J), hatched white lines outline the regenerating tissue exclusive of the epithelium. Error bars denote SEM. The scale bars in (A) and (J) represent 200 μm; (B) and (I) represent 20 μm; (C), (D), (K), and (L) represent 500 μm; and (J) (insets) represents 50 μm. See also Figure S3.

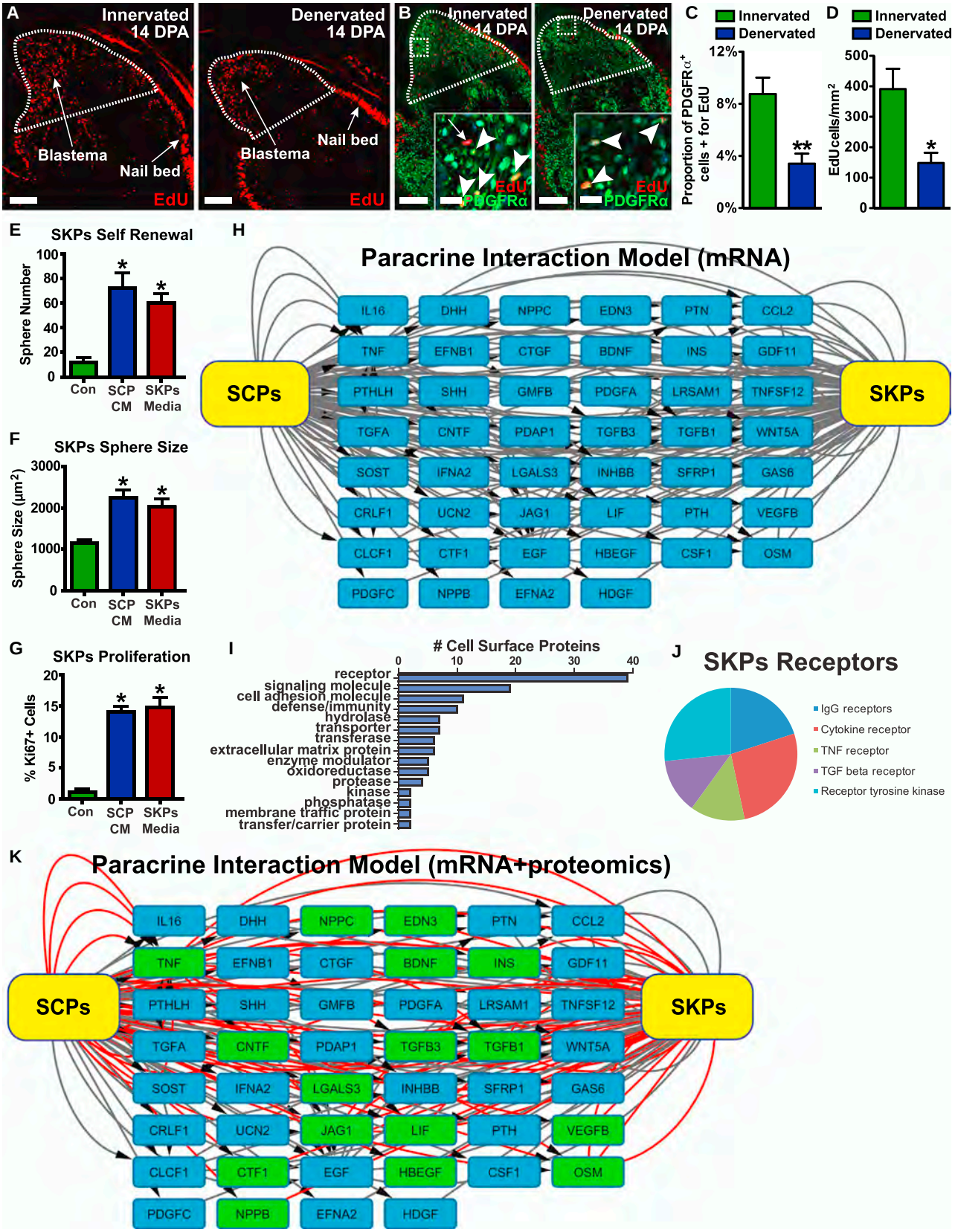

(legend on next page)

expression cutoff criteria. This analysis identified 121 potential SKP receptors (Table S3). We used this information to predict directional paracrine interactions from SCPs to SKPs (Figure 5H). This model identified 46 candidate SCP-secreted ligands (represented as nodes in the model) where the corresponding receptor was expressed on SKPs.

One disadvantage of a transcriptome-based model is that the correlation between mRNA abundance and protein expression levels is weaker for cell-surface proteins like growth factor receptors than for proteins in other compartments (Lundberg et al., 2010). We therefore characterized the cell surface proteome of cultured rat SKPs by performing periodate oxidation of cell-surface glycans (McDonald et al., 2009; Schiess et al., 2009), because most growth factor receptors are highly glycosylated. Coupled proteins were tryptically digested and glycopeptides released by PNGaseF and identified by mass spectrometry. For each sample, we analyzed three independent biological replicates. We identified 372 total proteins on SKPs (Table S4), and Gene Ontology (GO) analysis identified high enrichment for terms associated with the exterior of cells/vesicles as well as membrane-bound components, as predicted for cell surface proteins (Figure S4C; Table S5). Of these, 39 were classified as receptors and a further 30 as signaling and cell adhesion proteins using the protein analysis through evolutionary relationships (PANTHER) protein classification system (Figure 5I; Table S6). These receptors predominantly fell into five major categories, the immunoglobulin G (IgG) receptor superfamily, type 1 cytokine receptors, tumor necrosis factor (TNF) receptors, transforming growth factor β (TGF-β) receptors, and receptor tyrosine kinases (Figure 5J; Table S6).

We integrated the cell surface proteome data with our paracrine model by identifying receptors for all the ligands in our transcriptome model and overlapping these with the SKPs receptors identified in the cell surface proteome (Figure 5K). This validated 17 of the 46 ligands in our model, including the gp130 receptor ligand family members oncostatin M (OSM), leukemia inhibitory factor (LIF), ciliary neurotrophic factor (CNTF), and cardiotrophin 1 (CTF1), as well as two TGF-β family members, TGF-βs 1 and 3.

We asked whether these predicted factors might explain how SCPs promoted SKPs self-renewal, focusing on the gp130 cytokines and TGF-βs. We also tested PDGF-AA, which was predicted in the transcriptome model (Figure 5H), because its receptor, PDGFRα, was expressed in many blastema mesenchymal cells. We added each ligand individually to dissociated secondary passage rat SKPs with or without optimal SKPs growth factors. Quantification after 1 week showed that OSM and PDGF-AA both significantly increased SKP sphere numbers with or without fibroblast growth factor 2 (FGF2) and epidermal growth factor (EGF) (Figures 6A and 6B). Cardiotrophin-1 decreased SKP spheres in both conditions (Figures 6A and 6B) whereas TGF-β1 and TGF-β3 decreased SKP spheres only in the absence of FGF2 and EGF (Figure S5A). Notably, ELISAs confirmed that OSM and PDGF-AA were detectable in SCP-conditioned medium (Figures 6C and 6D), validating them as potential paracrine pro-regeneration factors.

OSM and PDGF-AA as Candidate Paracrine SCP Factors in the Regenerating Digit Tip

We next asked whether the potential paracrine communication pathways identified in the SCP/SKP interaction network model were also present in the regenerating digit tip blastema. We extracted RNA from three or four biological replicates each of the uninjured murine digit tip and of the regenerating adult digit tip blastema 2 weeks post-amputation and analyzed them on Mouse Gene 2.0 ST arrays. 1,745 genes were differentially expressed between these two groups ($p < 0.05$ false discovery rate [FDR]) with 516 at least 2-fold different (Figure 6E; Table S7; GEO: GSE81704). Unbiased hierarchical clustering (using the complete-linkage method) of a Euclidean distance matrix of $\log_2$ normalized expression data demonstrated that the replicates within each population clustered closely, validating the comparison (Figure 6E). Using the curated database, we found expression of 338 ligand mRNAs, with 314 similarly expressed in both groups. Six were 1.5- to 2-fold enriched in controls, and 18 were 2- to 25-fold enriched in the blastema (Figures 6F and 6G; Table S8). The most highly enriched in this latter group included those encoding PDGF-C, osteopontin (Spp1), angiopoietin 1 (Angpt1), and the TGF/bone morphogenetic protein (BMP) family members TGF-β1, TGF-β3, BMP1, and BMP4. The database also identified 348 total receptor mRNAs, with

Figure 5. Paracrine Network Analysis to Predict SCP Ligands that Promote Proliferation of Blastema Mesenchymal Precursor Cells

(A–D) *PDGFRα*$^{EGFP/+}$ mice that were or were not denervated were amputated, injected with EdU 13 DPA, and analyzed 1 day later. (A and B) Images of regenerating digits immunostained for EdU (red) and *PDGFRα*-EGFP (PDGFRα; green, B) and counterstained with Hoechst 33258 (blue, B) are shown. Hatched white lines denote the regenerating tissue exclusive of the epithelium. In (A), arrows denote the proliferative blastema and nail bed epithelium. In (B), the boxed regions in the blastema are shown at higher magnification in the insets. Arrowheads denote double-labeled cells and the arrow an EdU-positive, EGFP-negative cell in a small blood vessel. (C and D) Quantification of the regenerated digit tissue in images as in (B) for the proportion of *PDGFRα*-EGFP-positive cells that were also EdU-positive (C) and for the density of EdU-positive cells (D) is shown. *$p < 0.05$; **$p < 0.01$. n = 5 digits per group, two sections per digit.

(E–G) Secondary passage neonatal rat SKPs were cultured in defined medium that was conditioned by SCPs (SCP CM) for 7 days, and sphere number (E), size (F), and proportion of Ki67-positive proliferating cells (G) were quantified. As controls, SKPs were cultured in the same defined medium without conditioning (con) or in optimal SKPs medium containing FGF2 and EGF (SKPs media). *$p < 0.05$ by ANOVA with Dunnett's post hoc test; n = 4 biological replicates.

(H) Directional paracrine interaction model predictive of ligands secreted by SCPs that potentially regulate SKPs biology, constructed from transcriptome analysis of neonatal rat SCPs and SKPs. Ligands were considered if their $\log_2$ expression value was at least 50% of the top expression value in the SCP microarray dataset. The corresponding receptors were then identified in the SKP dataset and considered expressed if their $\log_2$ expression value was at least 50% of the top expression value. Only potential directional paracrine interactions from SCPs to SKPs are included, with each node showing an individual ligand that met these criteria.

(I–K) Cell-surface proteins on neonatal rat SKPs as identified by periodate oxidation of cell-surface glycans and mass spectrometry. (I and J) GO analysis in PANTHER of identified proteins that were annotated to the membrane in the Uniprot database, showing the number of proteins in each PANTHER protein class (I), is shown. The receptor class was further segmented to show relative proportions of the top receptor subclasses (J). (K) The paracrine SCP/SKPs model from (H), showing the 17 ligands whose receptors were identified on SKPs by the cell surface proteomic analysis (colored green), is shown.

Error bars indicate SEM. The scale bars in (A) and (B) represent 200 μm and (B) (insets) represents 20 μm. See also Figure S4.

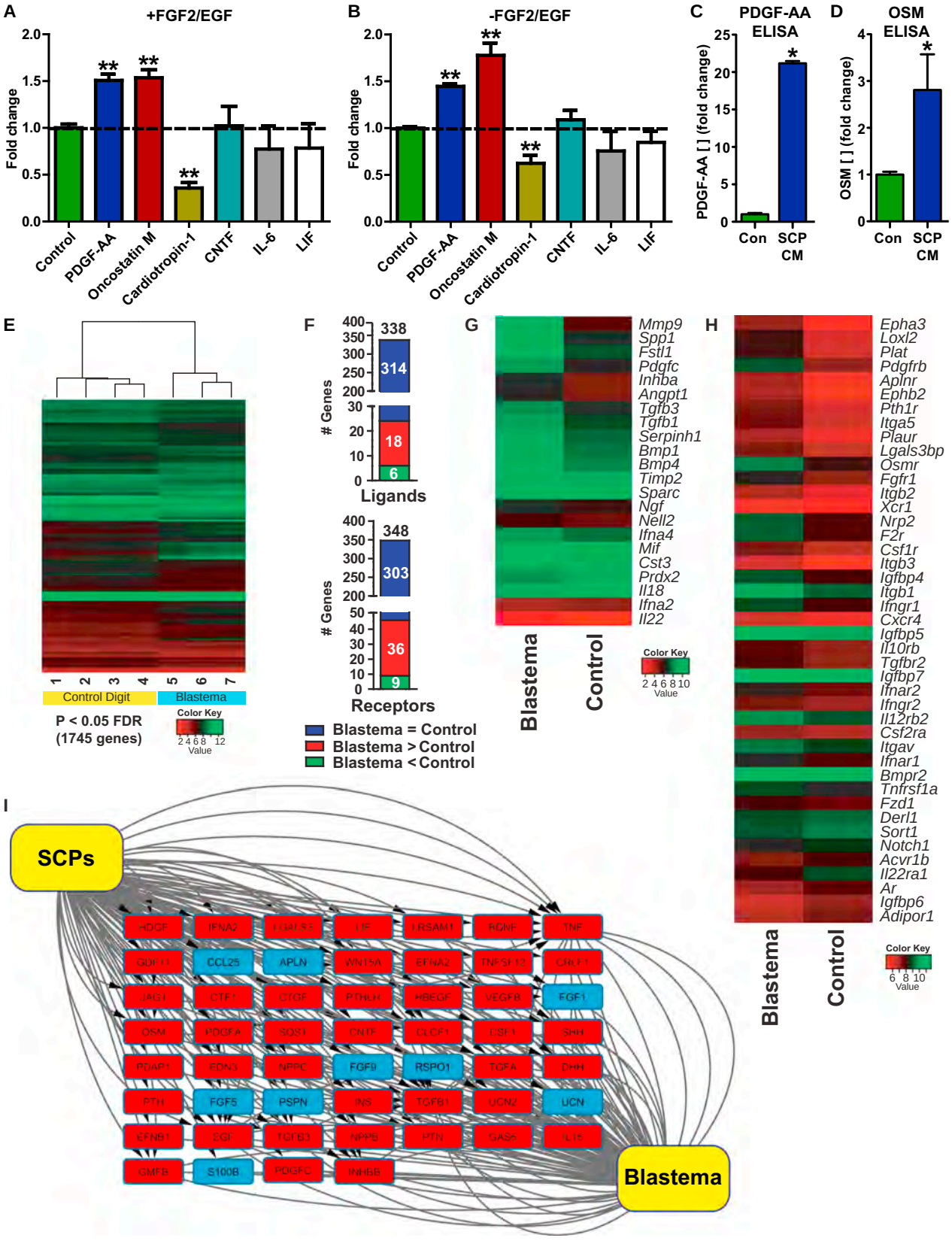

(legend on next page)

303 similarly expressed in both groups. Nine were 1.3- to 2-fold enriched in controls, and 36 were 1.3- to 4-fold enriched in the blastema (Figures 6F and 6H; Table S8), including OSM receptor β (*OSMRB*) mRNA.

We used the ligands expressed by SCPs and the receptors expressed in the blastema to predict potential directional paracrine interactions (Figure 6I). This model identified 53 candidate SCP ligands where the corresponding receptor was expressed in the blastema. Notably, there was very high overlap between the interactions predicted in this network and those predicted in the SCP/SKPs network (Figure 6I), with 46 potential ligands predicted in both networks, including OSM and PDGF-AA.

Local OSM or PDGF-AA Rescues the Denervation-Induced Deficit in Digit Tip Regeneration

To ask whether OSM and PDGF-AA were relevant for digit tip regeneration, we first confirmed by qRT-PCR that *OSM*, *PDGFA*, *OSMRB*, and *PDGFRA* mRNAs were all increased in the blastema relative to the uninjured digit (Figure 7A). We then used single molecule fluorescent in situ hybridization (FISH) and immunostaining to characterize their cellular localization. This analysis showed that *OSMRB* mRNA (Figure 7B) and gp130 (Figure 7C), the two components of the OSM receptor complex, were expressed in *PDGFRα*-EGFP-positive blastema cells and that *OSM* and *PDGFA* mRNAs were both expressed in S100β-positive SCPs (Figures 7D and 7E), although *PDGFA* mRNA was also expressed in other blastema cells. A time course analysis showed that S100β-positive SCPs expressed the highest levels of these two ligand mRNAs at 2 weeks, with a decrease to control levels when regeneration was complete at 4 weeks (Figures 7D–7G).

Having validated OSM and PDGF-AA as potential pro-regeneration ligands, we asked whether they could rescue the denervation-induced deficits in digit tip regeneration. We resected the sciatic nerve, amputated digit tips after 10 days, and, at 3 and 14 days post-injury, locally injected 200 ng of OSM or PDGF-AA. As negative controls, we injected denervated, amputated digits with vehicle alone. At 4 weeks, both bone and nail regeneration were impaired in denervated digits injected with vehicle alone, relative to regenerating innervated digits. In contrast, injection of either OSM or PDGF-AA was sufficient to rescue the denervation-induced deficits in regeneration (Figures 7H–7M, S6A, and S6B). However, in some animals injected with growth factors, morphology of the regenerated nail and bone were somewhat aberrant (see Figures 7H, 7I, S6A, and S6B), suggesting that the location of the secreted ligands relative to the blastema is important for patterning.

DISCUSSION

The distal digit tip provides one of the only examples of true multi-tissue regeneration in adult mammals. Here, we have defined an essential paracrine role for SCPs in digit tip regeneration, and on the basis of our data, we propose the following model. Following digit tip removal, axons distal to the lesion degenerate, thereby initiating dedifferentiation of their associated Schwann cells. These dedifferentiated SCPs localize to the regenerating blastema, where they secrete growth factors, most notably OSM and PDGF-AA, to promote expansion of blastema mesenchymal precursor populations. These mesenchymal precursors are necessary for regenerating tissues like the bone and dermis, and when blastema expansion is insufficient, regeneration is impaired. At later time points, axons regrow into the newly regenerated tissue, and the SCPs associate with these new axons and either differentiate back to a mature Schwann cell phenotype or maintain the NT SCP phenotype that we previously described (Johnston et al., 2013).

How does this model explain the effect of SCPs on nail regeneration? We propose that expansion of blastema mesenchymal precursors is necessary for nail regeneration, which involves recently identified epithelial stem cells (Lehoczky and Tabin, 2015), and is known to require signals from the underlying mesenchyme (Takeo et al., 2013). A similar inductive mechanism occurs during hair follicle morphogenesis, and the greater the number of inductive mesenchymal cells, the longer the resultant hairs (Biernaskie et al., 2009). By analogy, SCP-induced increases in blastema mesenchymal precursors would promote nail regeneration and deficits in blastema expansion would result in less nail regrowth.

Figure 6. Identification of OSM and PDGF-AA as Candidate Regeneration Factors by Transcriptome Modeling of the SCP/Blastema Paracrine Network

(A and B) Secondary passage neonatal rat SKPs were cultured in defined medium with (A) or without (B) FGF2 and EGF plus 100 ng/ml oncostatin M, cardiotrophin-1, leukemia inhibitory factor (LIF), interleukin-6 (IL-6), ciliary neurotrophic factor (CNTF), or PDGF-AA. Seven days later, SKP spheres were quantified and normalized to the medium without these added factors (other than FGF2 and EGF in A). Dotted lines show the control value of 1.0. $^{**}p < 0.01$ by unpaired two-tailed t test followed by Benjamini-Hochberg correction for false discovery; n = 4 biological replicates.

(C and D) ELISA for PDGF-AA (C) and OSM (D) in medium conditioned by SCPs, normalized to the same medium that was not conditioned. $^{*}p < 0.05$; n = 3.

(E–H) Microarray analysis was performed on three or four independent RNA preparations of the regenerating blastema 2 weeks post-amputation (blastema) and uninjured adult murine digit tips (control). (E) Heatmap and hierarchical clustering of all samples based on probe sets that differed by $p < 0.05$ (FDR) regardless of the fold-change when comparing the control digits and blastemas (1,745 in total) are shown. (F) Bar graphs showing the proportions of ligand-encoding genes (top graph) and receptor-encoding genes (bottom graph) identified in this analysis that were expressed at statistically similar levels in both groups (blue) or that were higher in the blastema (red) or higher in the uninjured digit tip (green). (G and H) Heatmaps of the ligand mRNAs (G) and receptor mRNAs (H) that were significantly differentially expressed between the blastema and control digit tips are shown. Heatmaps show the average value for all of the samples combined. In both cases, the genes most enriched in the blastema are on the top of the heatmap and those most enriched in the uninjured digit tip on the bottom.

(I) Directional paracrine interaction model predictive of ligands secreted by SCPs that could regulate the regenerating blastema, constructed from transcriptome analysis of SCPs and the blastema 2 weeks post-amputation. To construct this model, ligands were considered if their $\log_2$ expression value was at least 50% of the top expression value in the SCP microarray dataset. The corresponding receptors were then identified in the blastema dataset and considered expressed if their $\log_2$ expression value was at least 50% of the top expression value. Only potential directional paracrine interactions from SCPs to the blastema are shown, with each node showing an individual ligand that met these criteria. Red nodes indicate those ligands that are common between this network and the SCP/SKP paracrine model (Figure 5H).

Error bars indicate SEM. See also Figure S5.

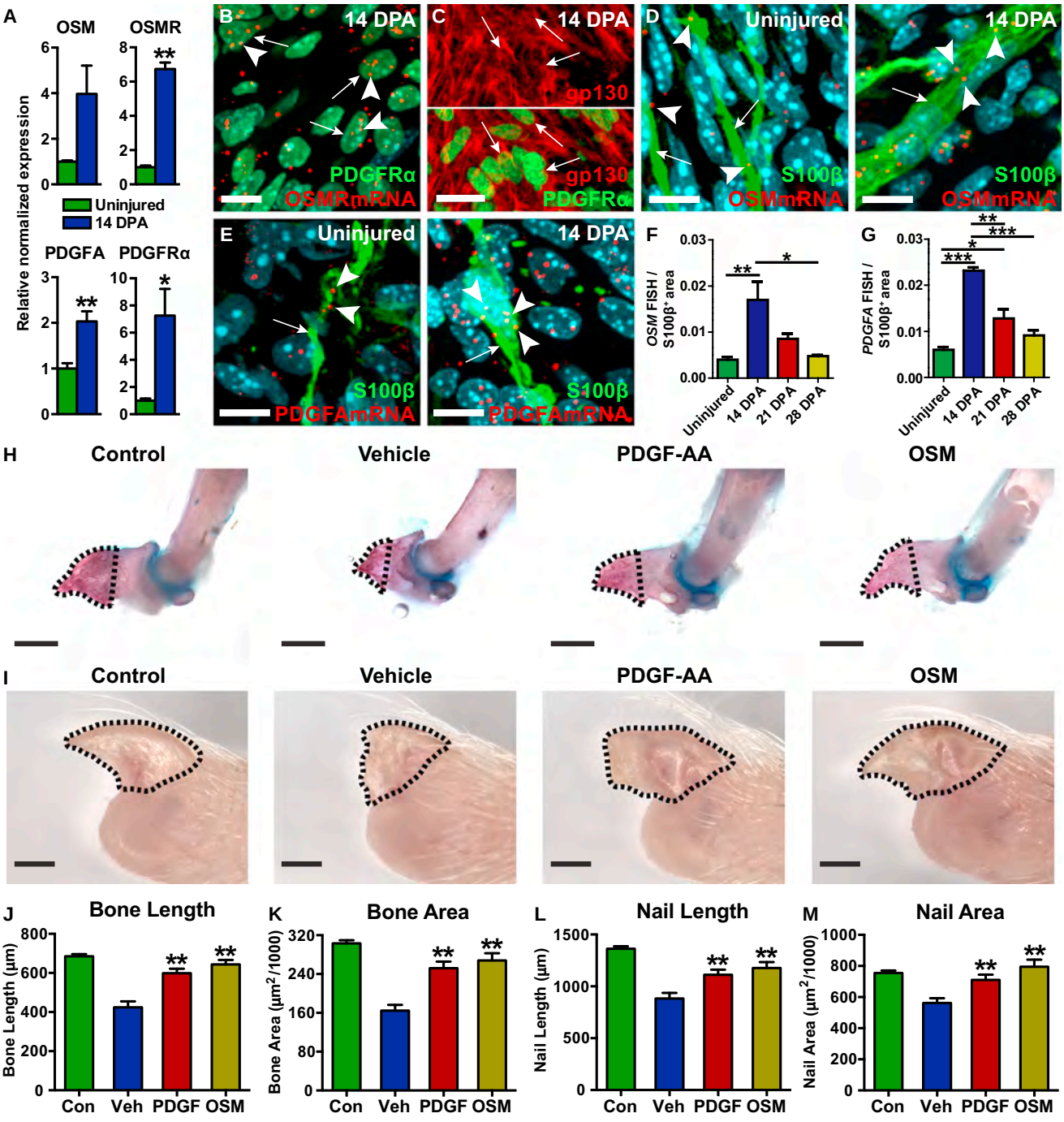

Figure 7. OSM and PDGF-AA Are Expressed by SCPs during Digit Tip Regeneration and Can Rescue the Denervation-Induced Regeneration Deficits

(A) qRT-PCR analysis of blastemas 2 weeks post-amputation, in comparison to uninjured digit tips. *$p < 0.05$; **$p < 0.01$; n = 3–4 independent samples per group. (B and C) Blastemas of *PDGFRα*-EGFP mice 14 DPA were analyzed by FISH for *OSMRB* mRNA (red dots; arrowheads; B) and immunostaining for *PDGFRα*-EGFP (PDGFRα, green) and gp130 (red, C). Arrows denote EGFP-positive cells that express *OSMRB* mRNA (B) or gp130 (C). In (C), the top and bottom images show the same field of view.

(D–G) Uninjured digit tips and regenerating digit tips at 14, 21, and 28 DPA were analyzed by FISH for *OSM* or *PDGFA* mRNAs and immunostaining for S100β. (D and E) Representative images of FISH for *OSM* mRNA (D; red dots; arrowheads) or *PDGFA* mRNA (E; red dots; arrowheads), coimmunostained for S100β (green) and counterstained with Hoechst 33258 (blue) are shown. Arrows denote EGFP-positive cells that express *OSM* or *PDGFA* mRNAs. (F and G) Quantification of images as in (D) and (E) for the density of FISH grains in S100β-positive SCPs. To perform this analysis, the total area of S100β-positive cells was measured with ImageJ and the number of *OSM* or *PDGFA* mRNA grains were expressed relative to this area measurement (in μm^2). *$p < 0.05$; **$p < 0.01$; ***$p < 0.005$ by one-way ANOVA with Tukey's post hoc analysis; n = 3 digits per group.

(legend continued on next page)

Our data are reminiscent of amphibian limb regeneration, where nerve innervation regulates the size of the regenerative blastema (Kumar et al., 2007; Rinkevich et al., 2014; Takeo et al., 2013). However, in amphibians, the nerve-derived pro-regenerative factor is thought to be anterior gradient protein (Ag1) (Kumar et al., 2007). Ag1 does not exist in mammals, but there are two other mammalian family members, Agr2 and Agr3 (Ivanova et al., 2013), which have been implicated in cancer, but not tissue repair (Obacz et al., 2015). Consistent with this, we have found no evidence for expression of Agr2 or Agr3 mRNAs in SCPs (data not shown). It will, however, be interesting to see whether OSM or PDGF-AA plays analogous roles during amphibian limb regeneration.

The identity of the PDGFRα-positive blastema precursors that respond to SCP-derived OSM and PDGF-AA is still an open question. The blastema includes diverse mesenchymal cells, including dermal cells, osteoprogenitor cells, and endothelial cells (Lehoczky et al., 2011; Rinkevich et al., 2011; Takeo et al., 2013). Our data show that many of these express OSMRβ, gp130, and PDGFRα and that at least one population, dermal mesenchymal precursors, responds directly to these growth factors. Whereas PDGF-AA regulates many mesenchymal precursors (reviewed in Andrae et al., 2008), little is known about OSM, although it can promote osteogenic differentiation of embryonic calvaria osteoprogenitors (Malaval et al., 2005), suggesting it might enhance both mesenchymal precursor proliferation and bone regeneration.

Our directional paracrine models suggest that SCPs secrete other ligands that might be important for digit tip regeneration. Among these are Wnt5A; Shh; Dhh; and FGFs 1, 5, and 9. Wnt activation is essential for digit tip regeneration (Takeo et al., 2013), and Hedgehog and FGF signaling have been implicated in amphibian regeneration (Makanae et al., 2016; Yakushiji et al., 2009). This is not to imply that SCPs are the only source of growth factors in the regenerating blastema. Indeed, our FISH studies show that *OSM* mRNA was predominantly expressed by SCPs but that *PDGFA* mRNA expression was more widespread. Moreover, BMP4, which has been implicated in neonatal digit tip regeneration (Han et al., 2008), was expressed in the blastema, but not predicted as an SCP paracrine factor. Thus, digit tip regeneration is likely to involve multiple growth factor sources, including SCPs.

These findings have broad implications for mammalian tissue repair. Our own work demonstrates that SCPs are essential for skin repair and digit tip regeneration, and other studies show that denervation inhibits repair of skeletal muscle (Pessina et al., 2014) and the heart (Mahmoud et al., 2015) and abolishes the enhanced regenerative capacity of the MRL mouse strain (Buckley et al., 2012). We propose that these deficits are due, at least in part, to loss of SCPs. Moreover, we propose that SCPs might be equally important in uninjured tissues, because *Sox2*-positive SCPs are located at NTs in the skin (Johnston et al., 2013), muscle (data not shown), and adult mouth palate (Widera et al., 2009). Thus, whereas it has long been known that SCPs secrete growth factors to promote peripheral nerve regeneration (Webber and Zochodne, 2010), these findings suggest that they play an equally crucial paracrine role in regulating tissue maintenance and regeneration outside of the nervous system.

EXPERIMENTAL PROCEDURES

Animals and Surgeries

This study was approved by the Hospital for Sick Children Animal Care Committee, in accordance with Canadian Council on Animal Care guidelines. Mice and rats were purchased from Charles River Laboratories. Details of transgenic mouse lines, tamoxifen treatment, and surgical procedures are in Supplemental Experimental Procedures.

Immunostaining

Immunostaining was performed on fixed cryosections, paraffin sections, or fixed cells as described (Johnston et al., 2013) with some modifications. Digital image acquisition was performed with a Quorum spinning disc confocal microscope using Volocity acquisition software (PerkinElmer) or on a Zeiss AxioImager M2 system. Further details and antibodies are in Supplemental Experimental Procedures.

Morphometric Analyses

Digital images of regenerated nails and distal bones were acquired with a Leica stereomicroscope and analyzed with Volocity acquisition software. For skin repair, H&E-stained paraffin sections from the central wound bed were analyzed as previously (Johnston et al., 2013). Further details are in Supplemental Experimental Procedures.

FISH Analyses

Single-molecule FISH was performed with the RNAscope kit (Advanced Cell Diagnostics) as per manufacturer's instructions, on cryosections of fixed, decalcified digits. Immunostaining was performed after FISH, z stacks of confocal images were acquired, and quantification performed using ImageJ and manual counting of FISH grains. Probes and further details are in Supplemental Experimental Procedures.

Cell Cultures and Conditioned Medium

SCPs were prepared from P1–P3 rat sciatic nerves as described previously (Krause et al., 2014). Secondary passage SKPs were prepared from P1–P3 rat back skin, and SKP sphere size, number, and proliferation were assessed as previously (Biernaskie et al., 2009; Naska et al., 2016). We also used the Operetta high-content imaging system (PerkinElmer) and CellProfiler (Version 2.1.1) for quantification in the growth factor experiments. PDGF-AA and OSM were measured using ELISA kits (R&D Systems and LS Bio, respectively). Further details are in Supplemental Experimental Procedures.

Microarray and qRT-PCR Analyses

RNA was isolated from SKPs and SCPs using the RNeasy kit (QIAGEN), or from blastemas and uninjured distal digits by homogenization in TRIzol (ThermoFisher), and purified with the RNeasy kit. RNA quality was assessed by an Agilent BioAnalyzer, and cDNA was generated with the Ambion Whole Transcript (WT) Expression Kit (Applied Biosystems) and analyzed on the Affymetrix GeneChip Mouse Gene 2.0 ST or Rat Gene 2.0 ST arrays. Details

(H–M) The sciatic nerves of adult mice were resected, 10 days later digit tips were amputated, 200 ng of OSM or PDGF-AA were injected immediately proximal to the injury site at 3 and 14 days, and regeneration was characterized 4 weeks post-amputation. As controls, normally innervated digit tips were amputated (con) or were denervated, amputated, and injected with vehicle alone (veh). (H and I) Representative images of the bone (H) or nails (I) of regenerated digits from all four groups are shown. Bones in (H) were stained with Alizarin red and Alcian blue, and nails (I) were imaged as whole mounts. Black hatched lines outline the regenerated tissues. (J–M) The extent of regeneration was quantified by measuring the length and area of the bone (J and K) and nail (L and M) from images as in (H) and (I). $^{**}p < 0.01$ by one-way ANOVA with Dunnett's post hoc analysis; n = 48 digits for control group and 15–21 digits per experimental group.
Error bars indicate SEM. The scale bars in (B), (D), and (E) represent 10 μm; (C) represents 20 μm; and (H) and (I) represent 500 μm. See also Figure S6.

of microarrays, qRT-PCRs, and primers are in Supplemental Experimental Procedures.

Cell-Surface Protein Analysis

Cell-surface mass spectrometry of secondary passage SKPs was performed as published (McDonald et al., 2009; Schiess et al., 2009) with minor modifications, using an Orbitrap analyzer (Q-Exactive; Thermo Fisher Scientific) outfitted with a nanospray source and EASY-nLC nano-LC system (Thermo Fisher Scientific). Data analysis, including MS1, label-free quantification, was performed with PEAK 7.5 software (Bioinformatics Solutions). GO analysis of cell-surface proteins was performed using the GOstats bioconductor package in R and PANTHER GO analysis (http://pantherdb.org). Further details are in Supplemental Experimental Procedures.

Computational Modeling

Ligands and receptors were identified using a curated database (Qiao et al., 2014; S.A.Y. and F.D.M., unpublished data). Details of modeling are in Supplemental Experimental Procedures.

Statistics

Except for microarray and proteomics analyses, statistics were performed with Student's t tests, one or two-tailed as appropriate, or ANOVA, if indicated in the text. Error bars indicate SEM.

ACCESSION NUMBERS

The accession number for the microarray data reported in this paper is GEO: GSE81704.

SUPPLEMENTAL INFORMATION

Supplemental Information includes Supplemental Experimental Procedures, six figures, and eight tables and can be found with this article online at http://dx.doi.org/10.1016/j.stem.2016.06.002.

AUTHOR CONTRIBUTIONS

A.P.W.J. conceptualized, designed, performed, and analyzed most of the experiments and co-wrote the paper. S.A.Y. and M.J.C. contributed equally to this manuscript. S.A.Y. conceptualized, designed, and analyzed the transcriptome and proteome analysis and paracrine modeling and co-wrote the paper. M.J.C. designed, performed, and analyzed many of the in vivo experiments and co-wrote the paper. N.M., M.A.S., M.P.K., and S.P. all designed, performed, and analyzed some of the experiments in the paper. K.J. helped establish the digit tip regeneration model. D.R.K. and F.D.M. conceptualized and designed experiments, analyzed data, and co-wrote the paper.

ACKNOWLEDGMENTS

This work was funded by CIHR grant MOP-64211 to F.D.M. F.D.M. and D.R.K. are Canada Research Chairs and F.D.M. is an HHMI Senior International Research Scholar. A.P.W.J. was funded by an Ontario Stem Cell Initiative fellowship, S.A.Y. and M.A.S. by Ontario Institute of Regenerative Medicine fellowships, M.J.C. by a CIHR MD/PhD studentship, and M.P.K. by a CIHR fellowship. We thank Molly Shoichet and Tobias Fuehrmann for their kind gift of HAMC. We thank Sevan Hopyan for advice and Benigno Aquino for technical assistance.

Received: February 1, 2016
Revised: May 10, 2016
Accepted: June 8, 2016
Published: June 30, 2016

REFERENCES

Andrae, J., Gallini, R., and Betsholtz, C. (2008). Role of platelet-derived growth factors in physiology and medicine. Genes Dev. *22*, 1276–1312.

Biernaskie, J., Paris, M., Morozova, O., Fagan, B.M., Marra, M., Pevny, L., and Miller, F.D. (2009). SKPs derive from hair follicle precursors and exhibit properties of adult dermal stem cells. Cell Stem Cell *5*, 610–623.

Borgens, R.B. (1982). Mice regrow the tips of their foretoes. Science *217*, 747–750.

Brockes, J.P., and Kumar, A. (2002). Plasticity and reprogramming of differentiated cells in amphibian regeneration. Nat. Rev. Mol. Cell Biol. *3*, 566–574.

Brownell, I., Guevara, E., Bai, C.B., Loomis, C.A., and Joyner, A.L. (2011). Nerve-derived sonic hedgehog defines a niche for hair follicle stem cells capable of becoming epidermal stem cells. Cell Stem Cell *8*, 552–565.

Buckley, G., Wong, J., Metcalfe, A.D., and Ferguson, M.W.J. (2012). Denervation affects regenerative responses in MRL/MpJ and repair in C57BL/6 ear wounds. J. Anat. *220*, 3–12.

Echeverri, K., and Tanaka, E.M. (2002). Ectoderm to mesoderm lineage switching during axolotl tail regeneration. Science *298*, 1993–1996.

Farahani, R.M., and Xaymardan, M. (2015). Platelet-derived growth factor receptor alpha as a marker of mesenchymal stem cells in development and stem cell biology. Stem Cells Int. *2015*, 362753.

Han, M., Yang, X., Lee, J., Allan, C.H., and Muneoka, K. (2008). Development and regeneration of the neonatal digit tip in mice. Dev. Biol. *315*, 125–135.

Ivanova, A.S., Tereshina, M.B., Ermakova, G.V., Belousov, V.V., and Zaraisky, A.G. (2013). Agr genes, missing in amniotes, are involved in the body appendages regeneration in frog tadpoles. Sci. Rep. *3*, 1279.

Johnston, A.P.W., Naska, S., Jones, K., Jinno, H., Kaplan, D.R., and Miller, F.D. (2013). Sox2-mediated regulation of adult neural crest precursors and skin repair. Stem Cell Reports *1*, 38–45.

Kirouac, D.C., Ito, C., Csaszar, E., Roch, A., Yu, M., Sykes, E.A., Bader, G.D., and Zandstra, P.W. (2010). Dynamic interaction networks in a hierarchically organized tissue. Mol. Syst. Biol. *6*, 417.

Kragl, M., Knapp, D., Nacu, E., Khattak, S., Maden, M., Epperlein, H.H., and Tanaka, E.M. (2009). Cells keep a memory of their tissue origin during axolotl limb regeneration. Nature *460*, 60–65.

Krause, M.P., Dworski, S., Feinberg, K., Jones, K., Johnston, A.P.W., Paul, S., Paris, M., Peles, E., Bagli, D., Forrest, C.R., et al. (2014). Direct genesis of functional rodent and human schwann cells from skin mesenchymal precursors. Stem Cell Reports *3*, 85–100.

Kumar, A., and Brockes, J.P. (2012). Nerve dependence in tissue, organ, and appendage regeneration. Trends Neurosci. *35*, 691–699.

Kumar, A., Godwin, J.W., Gates, P.B., Garza-Garcia, A.A., and Brockes, J.P. (2007). Molecular basis for the nerve dependence of limb regeneration in an adult vertebrate. Science *318*, 772–777.

Lehoczky, J.A., and Tabin, C.J. (2015). Lgr6 marks nail stem cells and is required for digit tip regeneration. Proc. Natl. Acad. Sci. USA *112*, 13249–13254.

Lehoczky, J.A., Robert, B., and Tabin, C.J. (2011). Mouse digit tip regeneration is mediated by fate-restricted progenitor cells. Proc. Natl. Acad. Sci. USA *108*, 20609–20614.

Lucas, D., Scheiermann, C., Chow, A., Kunisaki, Y., Bruns, I., Barrick, C., Tessarollo, L., and Frenette, P.S. (2013). Chemotherapy-induced bone marrow nerve injury impairs hematopoietic regeneration. Nat. Med. *19*, 695–703.

Lundberg, E., Fagerberg, L., Klevebring, D., Matic, I., Geiger, T., Cox, J., Algenäs, C., Lundeberg, J., Mann, M., and Uhlen, M. (2010). Defining the transcriptome and proteome in three functionally different human cell lines. Mol. Syst. Biol. *6*, 450.

Mahmoud, A.I., O'Meara, C.C., Gemberling, M., Zhao, L., Bryant, D.M., Zheng, R., Gannon, J.B., Cai, L., Choi, W.Y., Egnaczyk, G.F., et al. (2015). Nerves regulate cardiomyocyte proliferation and heart regeneration. Dev. Cell *34*, 387–399.

Makanae, A., Mitogawa, K., and Satoh, A. (2016). Cooperative inputs of Bmp and Fgf signaling induce tail regeneration in urodele amphibians. Dev. Biol. *410*, 45–55.

Malaval, L., Liu, F., Vernallis, A.B., and Aubin, J.E. (2005). GP130/OSMR is the only LIF/IL-6 family receptor complex to promote osteoblast differentiation of calvaria progenitors. J. Cell. Physiol. *204*, 585–593.

McDonald, C.A., Yang, J.Y., Marathe, V., Yen, T.-Y., and Macher, B.A. (2009). Combining results from lectin affinity chromatography and glycocapture approaches substantially improves the coverage of the glycoproteome. Mol. Cell. Proteomics *8*, 287–301.

Mohammad, K.S., and Neufeld, D.A. (2000). Denervation retards but does not prevent toetip regeneration. Wound Repair Regen. *8*, 277–281.

Naska, S., Yuzwa, S.A., Johnston, A.P.W., Paul, S., Smith, K.M., Paris, M., Sefton, M.V., Datti, A., Miller, F.D., and Kaplan, D.R. (2016). Identification of drugs that regulate dermal stem cells and enhance skin repair. Stem Cell Reports *6*, 74–84.

Neufeld, D.A., and Zhao, W. (1995). Bone regrowth after digit tip amputation in mice is equivalent in adults and neonates. Wound Repair Regen. *3*, 461–466.

Obacz, J., Takacova, M., Brychtova, V., Dobes, P., Pastorekova, S., Vojtesek, B., and Hrstka, R. (2015). The role of AGR2 and AGR3 in cancer: similar but not identical. Eur. J. Cell Biol. *94*, 139–147.

Pessina, P., Cabrera, D., Morales, M.G., Riquelme, C.A., Gutiérrez, J., Serrano, A.L., Brandan, E., and Muñoz-Cánoves, P. (2014). Novel and optimized strategies for inducing fibrosis in vivo: focus on Duchenne muscular dystrophy. Skelet. Muscle *4*, 7.

Qiao, W., Wang, W., Laurenti, E., Turinsky, A.L., Wodak, S.J., Bader, G.D., Dick, J.E., and Zandstra, P.W. (2014). Intercellular network structure and regulatory motifs in the human hematopoietic system. Mol. Syst. Biol. *10*, 741.

Rinkevich, Y., Lindau, P., Ueno, H., Longaker, M.T., and Weissman, I.L. (2011). Germ-layer and lineage-restricted stem/progenitors regenerate the mouse digit tip. Nature *476*, 409–413.

Rinkevich, Y., Montoro, D.T., Muhonen, E., Walmsley, G.G., Lo, D., Hasegawa, M., Januszyk, M., Connolly, A.J., Weissman, I.L., and Longaker, M.T. (2014). Clonal analysis reveals nerve-dependent and independent roles on mammalian hind limb tissue maintenance and regeneration. Proc. Natl. Acad. Sci. USA *111*, 9846–9851.

Schiess, R., Mueller, L.N., Schmidt, A., Mueller, M., Wollscheid, B., and Aebersold, R. (2009). Analysis of cell surface proteome changes via label-free, quantitative mass spectrometry. Mol. Cell. Proteomics *8*, 624–638.

Takeo, M., Chou, W.C., Sun, Q., Lee, W., Rabbani, P., Loomis, C., Taketo, M.M., and Ito, M. (2013). Wnt activation in nail epithelium couples nail growth to digit regeneration. Nature *499*, 228–232.

Toma, J.G., Akhavan, M., Fernandes, K.J., Barnabé-Heider, F., Sadikot, A., Kaplan, D.R., and Miller, F.D. (2001). Isolation of multipotent adult stem cells from the dermis of mammalian skin. Nat. Cell Biol. *3*, 778–784.

Webber, C., and Zochodne, D. (2010). The nerve regenerative microenvironment: early behavior and partnership of axons and Schwann cells. Exp. Neurol. *223*, 51–59.

Widera, D., Zander, C., Heidbreder, M., Kasperek, Y., Noll, T., Seitz, O., Saldamli, B., Sudhoff, H., Sader, R., Kaltschmidt, C., and Kaltschmidt, B. (2009). Adult palatum as a novel source of neural crest-related stem cells. Stem Cells *27*, 1899–1910.

Yakushiji, N., Suzuki, M., Satoh, A., Ide, H., and Tamura, K. (2009). Effects of activation of hedgehog signaling on patterning, growth, and differentiation in Xenopus froglet limb regeneration. Dev. Dyn. *238*, 1887–1896.

Yamazaki, S., Ema, H., Karlsson, G., Yamaguchi, T., Miyoshi, H., Shioda, S., Taketo, M.M., Karlsson, S., Iwama, A., and Nakauchi, H. (2011). Nonmyelinating Schwann cells maintain hematopoietic stem cell hibernation in the bone marrow niche. Cell *147*, 1146–1158.

Cell Stem Cell, Volume *19*

Supplemental Information

Dedifferentiated Schwann Cell Precursors Secreting Paracrine Factors Are Required for Regeneration of the Mammalian Digit Tip

Adam P.W. Johnston, Scott A. Yuzwa, Matthew J. Carr, Neemat Mahmud, Mekayla A. Storer, Matthew P. Krause, Karen Jones, Smitha Paul, David R. Kaplan, and Freda D. Miller

Supplemental Information

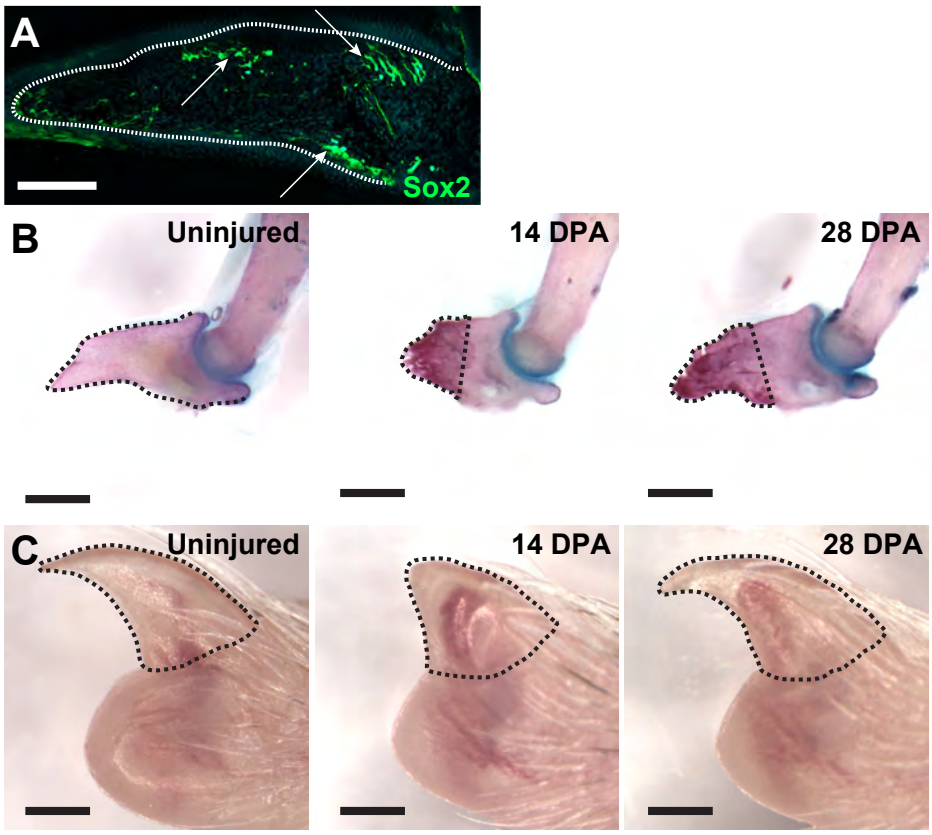

Supplemental Figure 1. ***Characterization of adult mouse digit tip regeneration.*** **Related to Figure 1.** (A) Confocal image of an uninjured distal digit from an adult *Sox2*$^{EGFP/+}$ mouse that was immunostained for EGFP (Sox2, green). The white hatched line in (A) outlines the digit, and arrows denote positive cells. This is the same image as shown in Fig. 1A, but at higher magnification. (B,C) Representative images of the distal bones (B) or nails (C) of regenerated digits from an adult mouse 14 or 28 days post-amputation (DPA). Shown for comparison are the bone and nail from a control, uninjured distal digit. Bones in (B) were stained with Alizarin red and Alcian blue, and nails (C) were imaged as whole mounts. The black hatched lines outline the regenerated bones and nails. Scale bars in A = 200μm; B, C = 500μm.

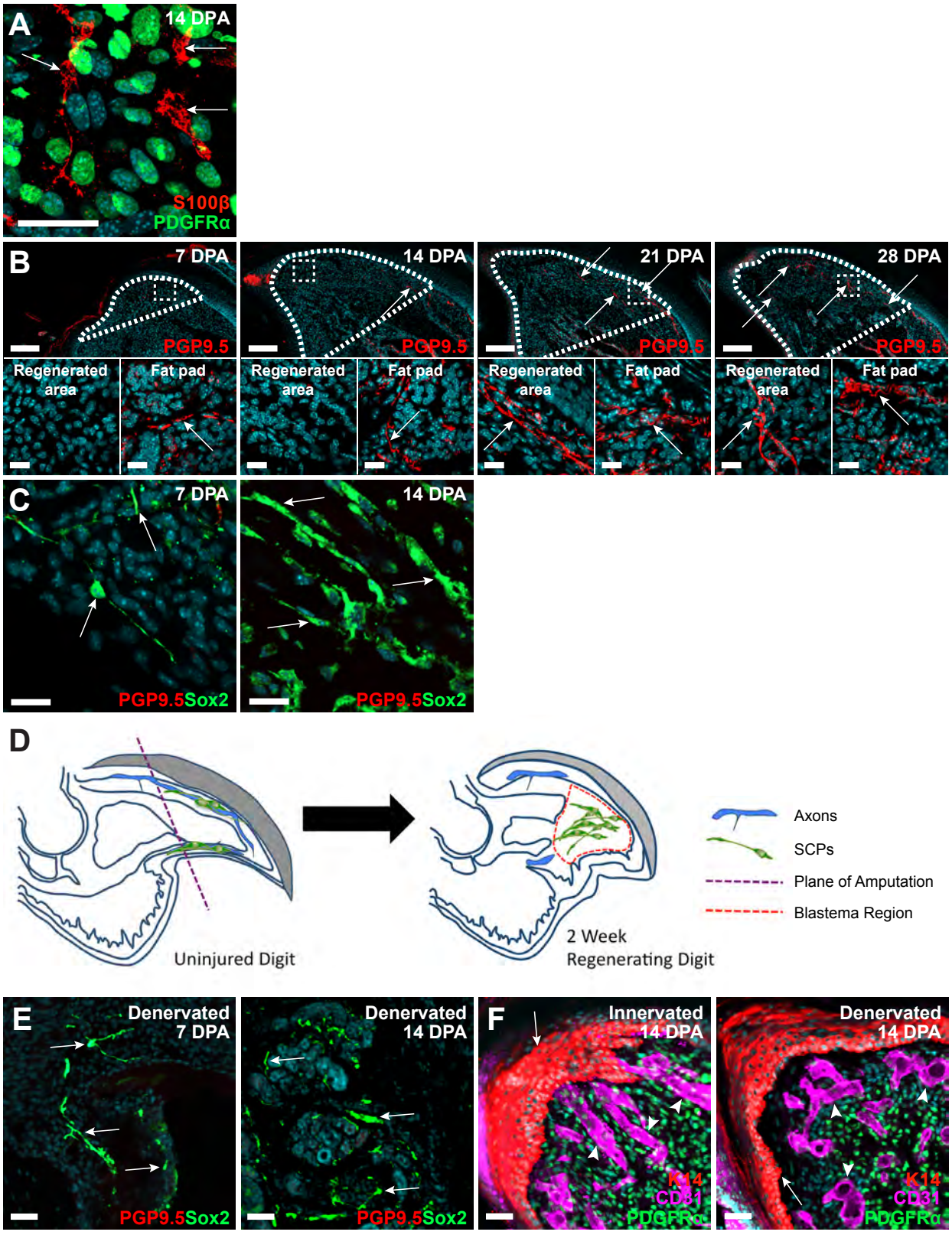

Supplemental Figure 2. ***Characterization of SCPs and axons in the control and denervated regenerating digit tip.*** **Related to Figure 2.** (A) Confocal image of the blastema of a

regenerating distal digit of an adult *PDGFRα*$^{EGFP/+}$ mouse 14 days post-amputation (DPA), immunostained for *PDGFRα*-EGFP (PDGFRα, green) and S100β (red). The arrows denote S100β-positive SCPs mingled with the blastema cells. (B) Confocal images of regenerating distal digits of adult mice at 7, 14, 21 and 28 days post-amputation (DPA), immunostained for Pgp9.5 (red) and counterstained with Hoechst 33258 (blue). The hatched white lines in the top images denote the regenerating tissue exclusive of the epithelium, and the boxed regions, which are located within the blastema at 7, 14 and 21 DPA, are shown at higher magnification in the bottom left images in each panel. For comparison, the bottom right images in each panel show Pgp9.5-positive axons within the adjacent fat pad, which is proximal to the amputation site. The arrows denote Pgp9.5-positive axons. (C) Confocal images of blastemas of regenerating digit tips from *Sox2*$^{EGFP/+}$ mice at 7 and 14 day post-amputation (DPA), immunostained for EGFP (green) and Pgp9.5 (red). Arrows indicate EGFP-positive SCPs that are not associated with Pgp9.5 axons. (D) Schematic showing the location of SCPs and axons in a regenerating digit at 2 weeks post-amputation. At this time point SCPs but not axons are present in the blastema. Axons are located proximal to the amputation plane and are largely absent from the regenerating digit tip. (E) Higher magnification images of digit tissue proximal to the amputation plane from sections of denervated, regenerating digits of *Sox2*$^{EGFP/+}$ mice at 7 and 14 days post-amputation (DPA), immunostained for EGFP (Sox2, green) and Pgp9.5 (red). These higher magnification images are from the same sections as shown in Fig. 2F. Arrows indicate *Sox2*-EGFP-positive SCPs. Note that there are no axons even in the proximal, uninjured digit tissue following a sciatic nerve resection. (F) Higher magnification confocal images of the blastema of regenerating distal digits of *PDGFRα*$^{EGFP/+}$ mice 14 days post-amputation (DPA) that had sham surgery (Innervated) or sciatic nerve resection (Denervated) 10 days prior to amputation, immunostained for *PDGFRα*-EGFP (PDGFRα, green), CD31 (purple) and K14 (red) and counterstained with Hoechst 33258 (blue). These images are from the same sections shown in Fig. 2G. Arrows denote the K14-positive epithelium and arrowheads the CD31-positive blood vessels in the regenerating digit. Scale bars in A, B (insets), C = 20μm; B = 200μm; E, F = 50μm.

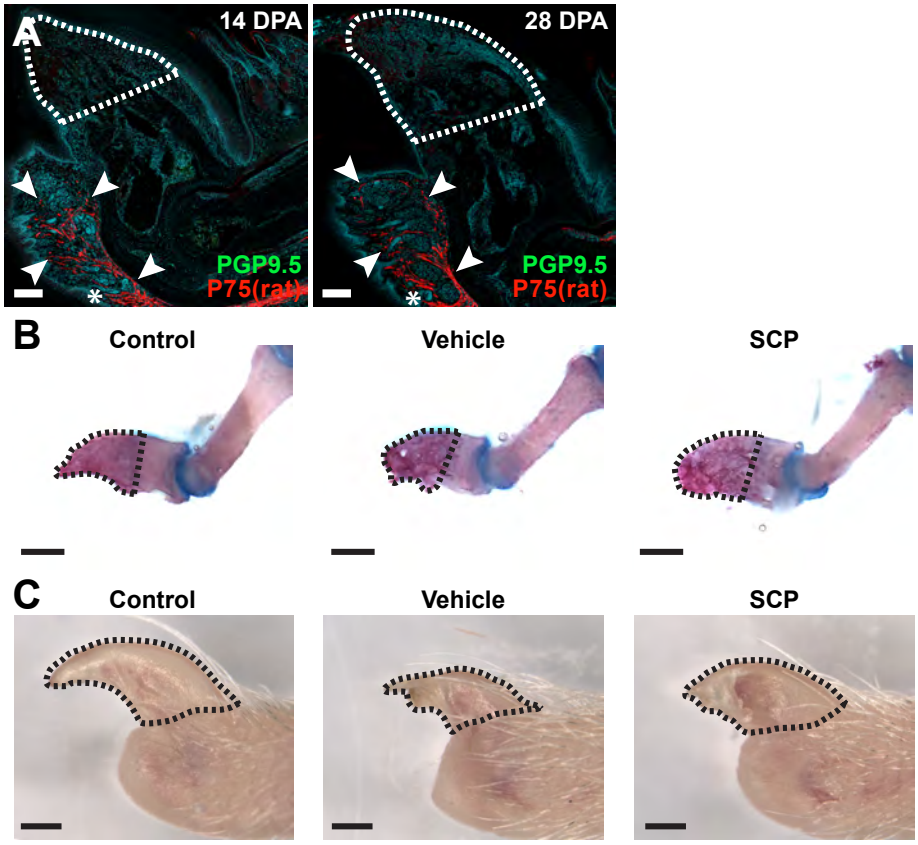

Supplemental Figure 3. ***Transplantation of exogenous SCPs rescues the denervation-induced deficits in digit tip regeneration.*** **Related to Figure 4.** Adult NOD-SCID mice were unilaterally denervated, ten days later ipsilateral digit tips were amputated, and 3 days later 500,000 rat SCPs were transplanted into the digit pad proximal to the amputation. As controls, mice were not denervated (Con) or were transplanted with the vehicle alone (Veh). (A) Confocal images of sections through denervated, regenerating digit tips at 14 and 28 days post-amputation (DPA) that were transplanted with SCPs, immunostained with an antibody specific for rat p75NTR (red) to detect transplanted cells, and Pgp9.5 to detect axons (green) and counterstained with Hoechst 33258 (blue). The hatched white lines show the regenerating digit tissue exclusive of the epithelium. The transplant site is indicated with an asterisk, and arrowheads denote p75NTR-positive transplanted rat cells. Note that no axons were seen in these sections. (B,C) Representative images of the bone (B) or nail (C) of regenerated digit tips from all three groups of mice at 4 weeks post-amputation. Bones in (B) were stained with Alizarin red and Alcian blue, and nails (C) were imaged as whole mounts. The black hatched lines outline the regenerated tissues. Scale bars in A = 200µm; B, C = 500µm.

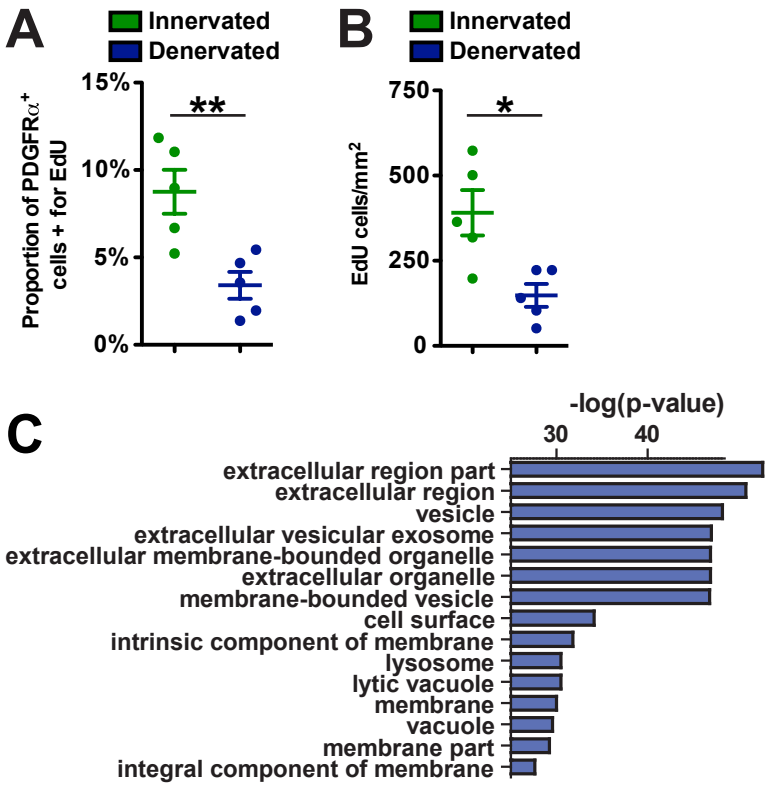

Supplemental Figure 4. ***SCPs secrete growth factors that regulate mesenchymal precursor proliferation.*** **Related to Figure 5.** (A,B) *PDGFRα*$^{EGFP/+}$ mice received sham surgery (Innervated) or sciatic nerve resection (Denervated), had their distal digits amputated 10 days later, were injected with EdU 13 days post-amputation, and analyzed one day later at 14 days post-amputation (DPA). Sections were immunostained for *PDGFRα*-EGFP and EdU and quantified for the proportion of *PDGFRα*-EGFP-positive cells within the regenerated tissue that were also EdU-positive (A) and the density of EdU-positive cells within the regenerated tissue (B). These scatter plots correspond to the bar graphs shown in Fig. 5C and D. *p<0.05, **p<0.01, n = 5 digits per group, 2 sections per digit. (C) GO (gene ontology) analysis of all SKP proteins identified by cell surface mass spectrometry, obtained using the GoStats package in R, showing enrichment for membrane-associated proteins.

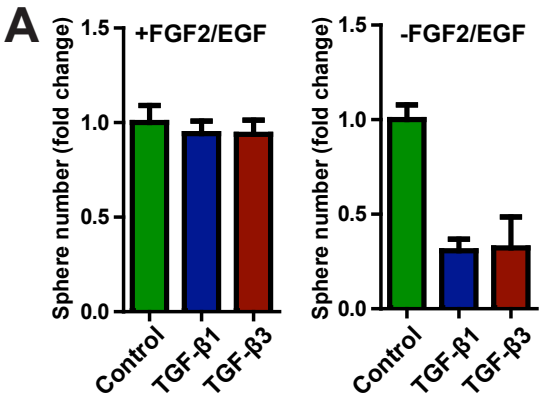

Supplemental Figure 5. ***Response of cultured SKPs to members of the TGF-β family*****. Related to Figure 6.** Secondary passage neonatal rat SKPs were cultured in defined medium with (left panel) or without (right panel) FGF2 and EGF plus 100 ng/ml TGF-β1 or TGF-β3. Seven days later the numbers of SKP spheres were quantified, and normalized to the medium without the added TGF-βs.

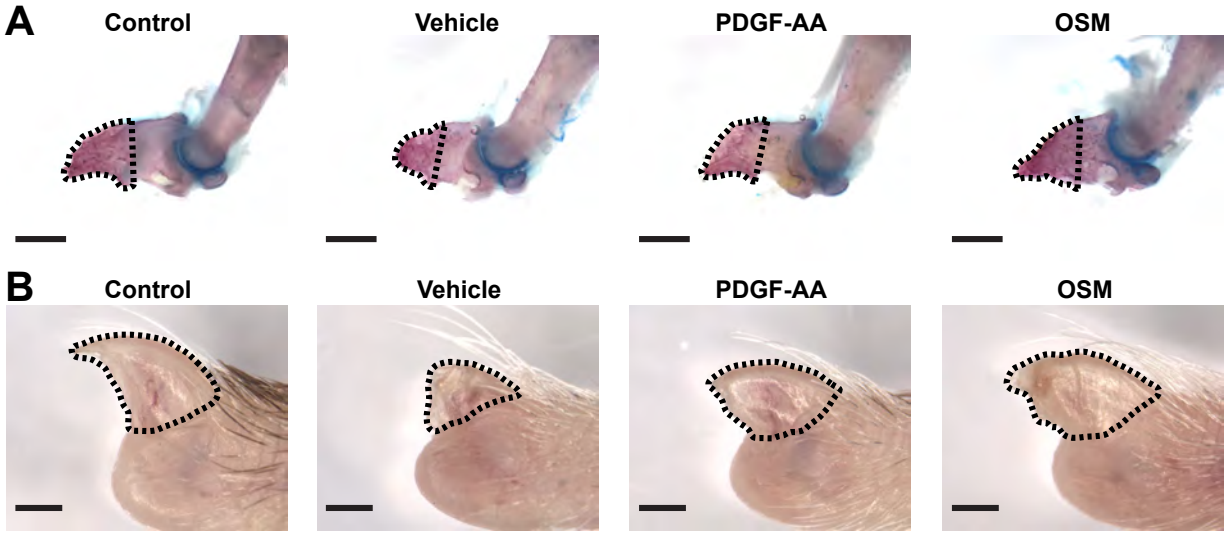

Supplemental Figure 6. ***OSM and PDGF-AA rescue the denervation-induced deficits in digit tip regeneration.*** **Related to Figure 7.** The sciatic nerves of adult mice were unilaterally resected, ten days later digit tips were amputated, 200 ng of OSM or PDGF-AA were then injected immediately proximal to the injury site at 3 and 14 days post-amputation, and regeneration was characterized 4 weeks post-amputation. As a positive control, normally innervated digit tips were amputated and allowed to regenerate for 4 weeks (Control) and as a negative control, denervated amputated mice were injected with vehicle alone and allowed to regenerate for 4 weeks (Vehicle). (A,B) Representative images of the bone (A) or nails (B) of regenerated digits from all four groups. Bones in (A) were stained with Alizarin red and Alcian blue, and nails (B) were imaged as whole mounts. The black hatched lines outline the regenerated tissues. Scale bars = 500μm.

Supplemental Table S1: ***RMA normalized log2-expression values for all annotated genes in the SKPs and SCPs microarray data.*** **Related to Figure 5.** RNA from three biological replicates of cultured rat neonatal SCPs and neonatal SKPs were analysed on Affymetrix Rat Gene 2.0 ST arrays. Raw probe intensity values were background corrected, normalized with quantile normalization, transformed into the $\log_2$ scale, and summarized into probesets with the RMA algorithm as described in the Experimental Methods section. Normalized data were then annotated using the 'ragene20sttranscriptcluster.db' bioconductor annotation package in 'R'. Shown here are $\log_2$ expression values for all annotated genes on the arrays, including the probe IDs (AffyProbeID), accession numbers, gene symbols (Symbol), descriptions and $\log_2$ expression levels from each biological replicate.

Supplemental Table S2: ***Ligand genes in the top 50% most highly expressed annotated genes in the SCPs microarray data.*** **Related to Figure 5.** RNA from three biological replicates of cultured rat SCPs was analysed on Affymetrix Rat Gene 2.0 ST arrays. Raw probe intensity values were background corrected, normalized with quantile normalization, transformed into the $\log_2$ scale, and summarized into probesets with the RMA algorithm as described in the Experimental Methods section. Normalized data was then annotated using the 'ragene20sttranscriptcluster.db' bioconductor annotation package in 'R'. Annotated data were ranked by the average $\log_2$ intensity for each annotated gene. Shown here are all ligand genes that were within 50% of the highest $\log_2$ expression value on the arrays, including the probe IDs (AffyProbeID), accession numbers, gene symbols (Symbol), descriptions and $\log_2$ expression levels from each biological replicate.

Supplemental Table S3: ***Receptor genes in the top 50% most highly expressed annotated genes in SKPs microarray data.*** **Related to Figure 5.** RNA from three biological replicates of cultured rat neonatal SKPs was analysed on Affymetrix Rat Gene 2.0 ST arrays. Raw probe intensity values were background corrected, normalized with quantile normalization, transformed into the $\log_2$ scale, and summarized into probesets with the RMA algorithm as described in the Experimental Methods section. Normalized data was then annotated using the 'ragene20sttranscriptcluster.db' Bioconductor annotation package in 'R'. Annotated data were ranked by the average $\log_2$ intensity for each annotated gene. Shown here are all ligand genes

that were within 50% of the highest log_2 expression value on the arrays, including the probe IDs (AffyProbeID), accession numbers, gene symbols (Symbol), descriptions and log_2 expression levels from each biological replicate.

Supplemental Table S4: ***All identified proteins from cell surface mass spectrometry of SKPs.*** **Related to Figure 5.** Cell surface proteins were prepared from three biological replicates of cultured neonatal rat SKPs (SKP1-3). All proteins detected by mass spectrometry in these preparations are shown here as identified by PEAKS 7.5 software. For each identified protein, in each biological replicate MS1 label-free quantitative values were calculated by PEAKS 7.5. Also shown for each identified protein are the description, average SKPs MS1 label-free quantitative value, accession number, the percent coverage, number of peptides, number of unique peptides and the identified post-translational modifications.

Supplemental Table S5: ***Cell surface proteins identified by cell surface mass spectrometry of SKPs.*** **Related to Figure 5.** Cell surface proteins were prepared from three biological replicates of cultured neonatal rat SKPs (SKP1-3). Shown here are proteins identified by mass spectrometry with PEAKS 7.5 software that were annotated as having cell surface or membrane bound sub-cellular localizations (in UniProtKB, uniprot.org). For each identified protein, in each biological replicate MS1 label-free quantitative values were calculated by PEAKS 7. Also shown are the average SKPs MS1 label-free quantitative values.

Supplemental Table S6: ***PANTHER protein classifications of all cell surface proteins identified by mass spectrometry.*** **Related to Figure 5.** All identified cell surface proteins from SKPs were classified into protein classes by the PANTHER gene-list classification system (pantherdb.org) using the rattus norvegicus annotations. Shown here are the UniportKB gene identification (Gene ID), the PANTHER mapped Ids (Mapped Ids), the gene name / gene symbol, the PANTHER protein class, the PANTHER 'Receptor' protein subclasses and species for each identified protein. In the PANTHER protein classifications, a number of receptor tyrosine kinases (such as *PDGFRB*, *INSR*, *FGFR1)* were not classified and we therefore manually added these unclassified proteins to the 'Receptor (PC00197)' classification as 'Receptor tyrosine kinase'.

Supplemental Table S7: ***Differentially-expressed genes with p < 0.05 FDR and any-fold change in control digit tips versus the two week regenerating blastema.*** **Related to Figure 6.** RNA from control murine digit tips and the 2 week regenerating blastema was analyzed on Affymetrix Mouse Gene 2.0 ST arrays, and differentially expressed genes were determined using the limma bioconductor package at the probeset level to generate $\log_2$ fold-change (shown here as inverse $\log_2$ fold-change) and moderated t-statistics (P-Value), and then annotated with mogene20sttranscriptcluster.db bioconductor annotation package for the gene symbol, description and accession number. Shown here are all annotated genes with p-values < 0.05 FDR and any fold-change.

Supplemental Table S8: ***Differentially-expressed ligand and receptor genes with p < 0.05 FDR and any-fold change in control digit tips versus the two week regenerating blastema.*** **Related to Figure 6.** RNA from control murine digit tips and the 2 week regenerating blastema was analyzed on Affymetrix Mouse Gene 2.0 ST arrays, and differentially expressed genes were determined using the limma bioconductor package at the probeset level to generate $\log_2$ fold-change (shown here as inverse $\log_2$ fold-change) and moderated t-statistics (P-Value), and then annotated with mogene20sttranscriptcluster.db bioconductor annotation package for the gene symbol, description and accession number. Shown here are all ligand and receptor genes that were found in a curated ligand and receptor database (Qiao et al., 2014; S.A.Y. and F.D.M., unpublished data) and their associated p-values and fold-changes.

Supplemental Experimental Procedures

Animals, tamoxifen, and surgeries. The following transgenic mouse strains were purchased from Jackson Laboratories: *Wnt1-Cre* (Tg(Wnt1-cre)11Rth Tg(Wnt1-GAL4)11Rth/J) (Danielian et al., 1998), *Sox2-CreERT2* (B6;129S-*Sox2*$^{tm1(cre/ERT2)Hoch}$/J) (Arnold et al., 2011), *R26-LSL-TdTomato* (B6;129S6-*Gt(ROSA)26Sor*$^{tm14(CAG-tdTomato)Hze}$/J) (Madisen et al., 2010), *PDGFRα*$^{EGFP/+}$ (B6.129S4-Pdgfrα $^{tm11(EGFP)Sor}$/J) (Hamilton et al., 2003), *R26-LSL-DTA* (B6;129-*Gt(ROSA)26Sor*$^{tm1(DTA)Mrc}$/J) (Wu et al., 2006). *Sox2*$^{+/EGFP}$ and *Sox2*$^{fl/fl}$ mice were maintained on a C57Bl/6J background and genotyped as previously described (Ellis et al., 2004; Taranova et al., 2006). Tamoxifen (Sigma) was dissolved in a sunflower oil/ethanol mixture (9:1) at 25 mg/ml. Vehicle or tamoxifen were injected intraperitoneally at 2.5mg/day for four consecutive days, as indicated in the results section. All injected mice were observed daily for any abnormalities. For denervation experiments, sciatic nerve resections were performed as previously described (Shao et al., 2007). Briefly, mice were anaesthetized with isoflurane gas, and a 5 mm incision was made into the lateral mid-thigh of the shaven hind right limb, through which the sciatic nerve was lifted and a 5 mm segment excised, before closing the wound with 4-0 Polysorb^{TM} sutures (Covidien, Saint-Laurent, QC). For analgesia, buprenorphine and ketoprofen were given subcutaneously at the time of surgery, and ketoprofen was re-administered after 24 h. Mice were allowed to heal for 10 days prior to performing digit amputations. Digit tip amputation experiments were performed as described previously (Simkin et al., 2013) using 10-12 week old mice that were anaesthetized and underwent amputation of the distal third of the terminal phalanges of the 2nd through 4th hind limb digits. Mice were given subcutaneous ketoprofen for analgesia immediately following digit amputation surgeries and were housed individually. For the skin repair experiments, 8-10 week old mice were anaesthetized, the dorsal hair was shaved and the exposed skin was cleaned with ethanol. Two 6 mm diameter full thickness excisional wounds were performed on each side of the dorsal midline using a biopsy punch (Miltex) as described previously (Johnston et al., 2013). Wounds were left uncovered and mice were given subcutaneous ketoprofen for analgesia and housed individually. For consistency, only one wound on the right dorsal side of each mouse was used for analysis (punch from outside to inside skin). Mice had free access to rodent chow and water in a 12 hour dark-light cycle room.

Cell transplantation and growth factor rescue experiments. For the cell transplantation experiments, SCPs were isolated from the sciatic nerves of P1-P3 neonatal Sprague-Dawley rats, then sorted and cultured as described below. Sciatic nerve denervation surgery, as outlined above, was performed on NOD-SCID mice, followed by digit tip amputations after 10 days. Cultured rat SCPs were released by trypsinization and resuspended in a vehicle of 1% hyaluronic acid and 1% methylcellulose (HAMC, kindly provided by Dr. Molly Shoichet). At 3 days post-amputation, mice were anaesthetized and a custom 30 gauge needle fitted to a 10 μl Microliter 700 Series Syringe (Hamilton Company, Reno, NV) was used to deliver a cell transplant of SCPs (500,000 cells per digit in 4 μl HAMC) or vehicle alone into the distal digit pad of denervated and amputated digits. For the growth factor rescue experiments, sciatic nerve resection was performed on C57Bl/6 mice, followed by digit amputation after 10 days. At 3 and 14 days post-amputation, mice were anaesthetized and received an injection of 200 ng recombinant murine PDGF-AA (Peprotech, Rocky Hill, NJ) or OSM (R&D Systems, Minneapolis, MN) (200 ng per digit in 4 μl HAMC) or vehicle alone. Subcutaneous ketoprofen was provided for analgesia at the time of transplantation. After 4 weeks, morphometric analysis of the extent of nail and bone regeneration were performed as described below. Separate mice receiving cell transplants were also analyzed at 1 day and 11 days following injection of cultured SCPs.

Tissue preparation and immunostaining. Freshly dissected digits were fixed in 4% PFA overnight at 4^{o}C followed by decalcification in 0.5M EDTA at pH 7.0 for 14 days at room temperature and cryosectioned coronally at 18 μm for immunostaining. For skin analyses, immunostaining was performed on cryosections while morphometric analyses and Ki67 staining were performed on paraffin sections, as previously described (Johnston et al., 2013). Briefly, wounds were fixed in 10% formalin, embedded in paraffin, bisected in the caudocranial direction, and serial sections from the central portion of the wound were immunostained with anti-Ki67 (1:100; LabVision) following antigen retrieval with citrate buffer. Primary antibodies were detected using the ABC kit and visualized using a DAB kit (both Vector Laboratories). For immunofluorescence of digit sections, slides were blocked with 5% BSA with 0.3% Triton-X100, while for skin cryosections, slides were blocked with 10% normal goat serum with 0.3% Triton-X100 and both were incubated with primary or secondary antibodies (overnight at 4^{o} C or at room temperature for 2 hours) followed by counterstaining with Hoechst 33258 (Sigma). In

cases where sections were incubated with anti-mouse antibodies, a MOM kit (Vector Laboratories) was used as per the manufacturer's instructions. For immunostaining of cultured cells, sorted SCPs were grown on 4 well chamber slides coated with poly-L-lysine (0.05%, Sigma) and laminin (15ug/ml, BD Biosciences). Upon reaching confluence the cells were fixed in 4% PFA. Cells were blocked with 5% BSA with 0.3% Triton-X100 and incubated with primary antibodies overnight at 4^{o} C and secondary antibodies for 1 hour at room temperature, followed by counterstaining with Hoechst 33258. Digital image acquisition was performed with a Quorum spinning disc confocal microscope using Volocity acquisition software (Perkin Elmer, Waltham, MA) consisting of a Olympus IX81 inverted fluorescence microscope (Center Valley, PA) equipped with a Hamamatsu C9100-13 back-thinned EM-CCD camera (Bridgewater, NJ). Primary antibodies used were chicken anti-GFP (1:1000; Abcam), rabbit anti-GFP (1:5000; Abcam), rabbit anti-p75NTR (1:500; Promega), mouse anti-rat P75NTR (1:500; Millipore), rabbit anti-Pgp9.5 (1:250; Ultraclone Ltd.), rabbit anti-Pgp9.5 (1:250; Cell Signalling), rabbit anti-RFP (1:1000, MBL), rabbit anti-S100β (1:500; Dako), goat anti-K14 (1:200; Santa Cruz), goat anti-CD31 (1:200; R & D Systems), rat anti-CD31 (1:200; BioLegend), mouse anti-gp130 (1:200; Santa Cruz), mouse anti-rat nestin (1:500; BD Pharmingen), goat polyclonal Sox-2 (Y-17) (1:500; Santa Cruz). Secondary antibodies were anti-rabbit, rat, mouse, human, goat, or chicken Alexa-488, 555 or 647 (1:1000; Molecular Probes) or Cy3-conjugated streptavidin (Jackson Immuno Research Laboratories).

S100β quantification. To quantify SCPs within the regenerated tissue, fluorescent images of digit tip sections imunostained with S100β and counterstained with Hoechst 33258 (Sigma) were acquired on a Zeiss AxioImager M2 system equipped with an X-cite 120 LED light source and a C11440 Hamamatsu camera. ImageJ analysis software (Bethesda, MD) was used to trace outlines of the regenerated regions and quantify their areas. Positive cells were manually identified, only counting S100β-positive cells associated with a nucleus by Adobe Photoshop (Adobe Systems Incorporated). Three sections per digit were analysed, averaged, and then these were combined with other digits for statistical analysis.

EdU labelling and analyses. Mice were injected with 100mg/kg 5-Ethynyl-2'-deoxyuridine (EdU) (Molecular Probes) intra-peritoneally 1 day prior to analysis. EdU was detected using the

Click-iT Alexa Fluor 555 imaging kit (Thermo Fisher) as per the manufacturer's instructions. To quantify proliferating cells within the regenerating digit tip, digital images of sections immunostained for EdU and the mesenchymal marker PDGFRα-EGFP were obtained and the region corresponding to the blastema outlined and measured using ImageJ analysis software (Bethesda, MD). The density of EdU-positive cells and percentage of EdU+/PDGFRα-EGFP double positive cells was determined by manual counting using Adobe Photoshop (Adobe Systems Incorporated). Two sections per digit were analysed, averaged, and then these were combined with other digits for statistical analysis.

Morphometric analyses. To quantify nail length and area, digital images of freshly dissected nails were taken on a Leica fluorescence stereomicroscope (Buffalo Grove, IL) equipped with a Micropublisher 5.0 RTV colour camera and a Plan-Apo 1x objective lens, operated by Volocity acquisition software. ImageJ analysis software (Bethesda, MD) was used to trace outlines of the regenerated nails and measure length and area. For bone analysis digits were subjected to skeletal staining as previously described (Ovchinnikov, 2009). Briefly, digits were soaked in 1M NaCl at room temperature for 12-24 h to facilitate removal of cutaneous tissues and nail, then dehydrated in 95% ethanol for 24 h prior to staining in 0.03% Alcian Blue 8GX solution (Sigma) for 24 h. Digits were washed in 95% ethanol and then stained for 4 h in 0.03% Alizarin Red S (Sigma) before final clearing for 5-7 days in a 20% glycerol/1% KOH solution. The regenerated distal phalanges were imaged and quantified as described above for nail quantification. Morphometric analyses of skin repair parameters were performed on hematoxylin and eosin-stained paraffin tissue sections from the central portion of the wound bed. Sections were scanned using 20x/0.75 lens (Zeiss Mirax Scan) and were stitched together using the Mirax Scan software. Morphometric analysis were performed as described previously (Martin et al., 2010), using Northern Eclipse software (Empix). Briefly, epithelial gap was measured as the distance between the new epithelial tongues. Wound width was measured as the distance between the wound margins which were defined by the last hair follicles and wound area was measured on digital images using ImageJ. The number of Ki67 positive cells in the new dermal tissue was determined by counting the total number of Ki67 positive cells within the regenerating dermis using Adobe Photoshop (Adobe Systems Incorporated).

Fluorescent in situ hybridization analyses. Single molecule FISH was performed using the RNAscope kit (Advanced Cell Diagnostics) according to manufacturer's instructions, with probes targeting *OSM* (NM_001013365.2; cat# 427071-C2), *PDGFA* (NM_008808.3; cat# 411361-C2), and the *OSMRβ* (NM_011019.3 cat# 427081). Briefly, freshly dissected regenerating digits were fixed overnight in 4% PFA followed by decalcification at room temperature for 14 days in 0.5M EDTA at pH 7.0 and then cryosectioned coronally at 14 µm. Sections were washed with ethanol, followed by tissue pretreatment (1:10 dilution), probe hybridization and signal amplification. Positive staining was identified as punctate dots. Z-stacks of confocal images were taken with optical slice thickness of 0.3 µm, and projected Z-stacked images were shown. Immunostaining was performed following completion of FISH as described above. For quantification of *OSM* and *PDGFA* FISH, sections were processed for FISH and then immunostained for S100β. The total S100β immunoreactive area was measured by manually outlining the S100β immunostaining in ImageJ. The numbers of *OSM* or *PDGFA* FISH punctae within the outlined areas were counted and the data were expressed as the density of *OSM* or *PDGFA* punctae per S100β-positive area (in μm^2).

Cell cultures and conditioned medium experiments. SCPs were isolated from neonatal rat sciatic nerves, cultured and sorted as described previously (Krause et al., 2014). Briefly, sciatic nerves of neonates were dissected and digested in collagenase type XI (1 mg/ml, Sigma) at 37°C for 30 min. Cells were resuspended in medium containing DMEM/F12 (3:1, Invitrogen), 5% fetal bovine serum (FBS), 1% penicillin/streptomycin (P/S), 2% N2 supplement (Invitrogen), 25 ng/ml neuregulin-1β (R&D Systems), 5 µM forskolin (Sigma) and cultured on coated plates (4 µg/ml laminin [BD Biosciences], 30 µg/ml poly-D-lysine hydrobromide). To purify SCPs, cells were incubated in conditioned medium containing Necl1-Fc coupled to 488-conjugated anti-human IgG at 37^{o}C for 30 min (Krause et al., 2014). Cells were then washed in PBS and collected using 0.5% trypsin EDTA and sorted using a MoFlo (Dako, Glostrup, Denmark). Thereafter, SCPs were grown in basal SCP growth medium containing 1% P/S, 2% N2 supplement (Invitrogen), 25 ng/ml neuregulin-1β (R&D Systems) and 5 µM forskolin (Sigma) on coated plates.

SKPs were isolated from the back skin of P1-P3 neonatal Sprague-Dawley rats, as previously described (Biernaskie et al., 2006, 2009; Fernandes et al., 2004). Briefly, skin was

dissected and cut into 1-2 mm pieces and incubated in collagenase type XI (Sigma) for 30 min at 37°C. Samples were centrifuged, the supernatant was removed, and tissue pieces were resuspended in DMEM/F12 medium, (3:1, Invitrogen) containing 1% penicillin/streptomycin and manually dissociated by pipetting. Cells were cultured at 50,000 cells/ml in SKPs basal growth medium (DMEM-F12, 3:1 and 40 ng/ml FGF2 (Peprotech), 20 ng/ml EGF (BD Biosciences), 2% B27 (Invitrogen), and 1 µg/ml fungizone (Invitrogen) and allowed to form spheres. Second passage SKPs, dissociated by incubation with collagenase type XI (Sigma) were used for all experiments, unless otherwise indicated. For conditioned medium experiments, dissociated SKPs were plated at a density of 5000 cells per well of a 96 well plate in SKPs basal growth medium, basal SCP growth medium or SCP growth medium that had been conditioned for 5-7 days by sorted SCPs. Sphere size and number were assessed by counting using an upright light microscope (Olympus). To quantify the proportion of of Ki67-positive cells, SKPs were grown under conditions described above and were cytospun onto slides and immunostained with anti-Ki67 (Abcam, 1:500). The number of Ki67 positive cells per total number of Hoechst 33258-positive cells was quantified through manual counting in a blinded fashion of 3 biological replicates.

High-content analysis. For the growth factor experiments SKPs were prepared as described above and plated at a density of 5000 cells/well in optically clear bottom 96 well plates (Nunc, CellCarrier^{TM} – 96) in SKPs basal medium. Immediately following plating, cells were treated with rat PDGF-AA, OSM, CT-1, CNTF, LIF, IL6, TGF-β1 or TGF-β (all Peprotech) at 100 ng/ml for 7 days. Cells were then fixed with 4% PFA and stained with Hoechst 33258 to visualize spheres. 20 images of Hoechst-stained fields were collected per well using an Operetta high-content imaging system (PerkinElmer) and the number of spheres were quantified using CellProfiler (Version 2.1.1 (Carpenter et al., 2006) with an analysis pipeline that contained "IdentifyPrimaryObjects" modules. Spheres of between 30 and 100 pixel units were counted using an adaptive background strategy. Following object identification, CellProfiler data was output to comma separated values files where the data was further analyzed to calculate sphere number.

qRT-PCR analyses. 10 µL PCR reaction mixture containing FastStart DNA Master SYBR Green I (Roche Molecular Biochemicals) was prepared according to the manufacturer's instructions, and loaded on to a 96 multiwell plate. The CFX96 thermocycler (Bio-Rad) was used with a protocol involving an initial activation cycle (2 min, 95°C), 45 cycles of denaturation (10 sec, 95°C), annealing (20 sec, 60°C) and elongation (20 sec, 72°C). A single fluorescence reading was acquired at the end of each elongation step. A melting curve analysis cycle was performed after the PCR amplification. The primers used for qRT-PCR were: *PDGFA* forward 5'-TGTGCCCATTCGCAGGAAG-3' and reverse 5'-GAGGTATCTCGTAAATGACCGTC-3', *PDGFRα* forward 5'-TCCATGCTAGACTCAGAAGTCA-3' and reverse 5'-TCCCGGTGGACACAATTTTTC-3', *OSM* forward 5'-CAGAATCAGGCGAACCTCACG-3' and reverse 5'-AGCTCTCAGGTCAGGTGTGTT-3', *OSMR* forward 5'-GCATCCCGAAGCGAAGTCTT-3' and reverse 5'-GGGCTGGGACAGTCCATTCTA-3', and *β-tubulin* forward 5'-GACAGAGGCAAACTGAGCACC-3' and reverse 5'-CAACGTCAAGACGGCCGTGTG-3' (Invitrogen). All primers for qRT-PCR were validated in accordance with MIQE guidelines (Bustin et al., 2009).

Microarray analysis. Three biological replicates each of neonatal rat secondary passage SKPs and expanded SCPs were prepared as above and RNA isolated using the RNeasy kit (Qiagen). Alternatively, uninjured distal right digits or blastemas dissected from distal right digits of C57Bl/6 mice 2 weeks post-amputation were homogenized in TRIzol (ThermoFisher), and RNA purified with the RNeasy kit. RNA quality was assessed by an Agilent BioAnalyzer, cDNA was generated with the Ambion Whole Transcript (WT) Expression Kit (Applied Biosystems) and was analyzed on the Affymetrix GeneChip Mouse Gene 2.0 ST or Rat Gene 2.0 ST arrays. The hybridized microarray image was scanned with the GeneChip Scanner 3000 7G (Affymetrix). Raw probe intensity values were background corrected, normalized with quantile normalization, transformed into the $\log_2$ scale, and summarized into probesets using the Robust Multichip Analysis (RMA) algorithm using the Oligo bioconductor package in R (Carvalho and Irizarry, 2010). To calculate differential gene expression, the limma bioconductor package was used to calculate Bayesian statistics. In these analyses, any annotated gene with an expression change of $p < 0.05$ FDR (Benjamini and Hochberg correction) was considered statistically significant. For the hierarchical clustering and heatmap analysis, all of the genes with $p < 0.05$ FDR when

comparing the control digit and regenerating blastema were used to perform the cluster and heatmap analysis using the heatmap.2 function of the gplots package in R. In this case, the complete linkage method of a Euclidian distance matrix was used to perform the cluster analysis. Gene Ontology (GO) analysis was performed using the GOstats bioconductor package in R. The gene 'universe' in this analysis was all of the mapped keys in the org.Mm.egGO and org.Ra.egGO databases for the Mouse Gene 2.0 ST and Rat Gene 2.0 ST arrays, respectively, while the differentially expressed genes (computed as described above) served as the enrichment samples. The threshold p-value in the GO analysis was set at $p < 0.001$.

Cell Surface Protein Analysis. Cell surface mass spectrometry of secondary passage SKPs was carried out as published (McDonald et al., 2009; Schiess et al., 2009) with slight modifications, as follows. SKPs were isolated as described above and secondary passage spheres were generated. Five T75 flasks were combined, the media removed, and cells were washed once with coupling buffer (1x PBS pH 6.5, 0.1% FBS) then treated with 5 ml of 5 mM $NaIO_4$ in coupling buffer for 30 minutes at room temperature in the dark. Cells were then washed twice with PBS and lysed in buffer containing 20 mM Tris-HCl, 150mM NaCl , 0.0002% NaN_3 , 1% NP-40, pH 7.5 and one complete-mini protease inhibitor tablet per 10 ml of lysis buffer. Lysates were passed through 23-gauge needles. Protein lysates were added to 200 µl of Ultralink Hyrdazide resin (Pierce) pre-equilibrated with lysis buffer and rotated overnight at room temperature. The following day, the unbound protein was removed via centrifugation, washed twice with 8M urea and three times with 50 mM ammonium bicarbonate (pH 8, ABC). The resin was then treated with 50 mM dithiothreitol (DTT, American Bioanalytical) in ABC at 37 ºC for 60 minutes, washed once with ABC and then incubated with 65 mM iodacetamide in ABC at room temperature in the dark for 30 minutes. The resin was then washed once with ABC, once with 1.5 M NaCl and three times with ABC and finally incubated with 40 ng/µl of trypsin (Worthington) in ABC overnight at 37 ºC. The following day, the resin was washed three times with 1.5 M NaCl, three times with 80% acetonitrile, three times with methanol, three times with water, three times with ABC and finally incubated with 1300 units / ml of PNGAseF (New England Biolabs) at 37 ºC overnight in ABC. The following day, the eluted peptides were collected from the resin and the resin was washed once with ABC and combined with the eluted peptides. The eluates were then lyophilized overnight and prepared for mass spectrometry using

C18 reverse-phase ZipTips® (EMD Millipore). Following elution from ZipTips®, peptides were lyophilized and resuspended in 11µL of 0.1% formic acid. Samples were analyzed on a Orbitrap analyzer (Q-Exactive, Thermo Fisher) outfitted with a nanospray source and EASY-nLC nano-LC system (Thermo Fisher). 5µL / sample was loaded onto a 75µm x 50cm PepMax RSLC EASY-Spray column filled with 2 µM C18 beads (Thermo Fisher) at a pressure of 800 Bar. Peptides were eluted over 60 min at a rate of 250 nl/min using a 0 to 35% acetonitrile gradient in 0.1% formic acid. Peptides were introduced by nano-electrospray into the Q-Exactive mass spectrometer. The instrument method consisted of one MS full scan (400–1500 m/z) in the Orbitrap mass analyzer with an automatic gain control (AGC) target of 1e6, maximum ion injection time of 120 ms and a resolution of 70,000 followed by 10 data-dependent MS/MS scans with a resolution of 17,500, an AGC target of 1e6, maximum ion time of 120ms, and one microscan. The intensity threshold to trigger a MS/MS scan was set to 1.7e4. Fragmentation occurred in the HCD trap with normalized collision energy set to 27. The dynamic exclusion was applied using a setting of 20 seconds. Data was analyzed in PEAK 7.5 software (Bioinformatics Solutions Inc.). MS1, label-free quantification of identified proteins was calculated by Peaks 7.5 software. Gene Ontology (GO) analysis of cell surface proteins was performed using the GOstats bioconductor package in R. The gene 'universe' in this analysis was all of the mapped keys in the org.Ra.egGO database, while all identified proteins in the cell surface mass spectrometry preparations served as the enrichment samples. The threshold p-value in the GO analysis was set at $p < 0.001$. PANTHER GO analysis (pantherdb.org) was used to classify cell surface proteins into PANTHER protein classes.

Computational modeling. Microarray data were processed as described above to produce RMA normalized $\log_2$ expression data. Expression data for each annotated gene for the three biological replicates of SCPs, SKPs or injured digits was then averaged. Computational modeling was then carried out as described previously (Kirouac et al., 2010) with minor modifications as implemented in Python (Version 2.7.6, code available upon request). Briefly, the maximum average $\log_2$ expression value for each annotated gene in the SCP, SKPs or blastema data was determined and a value which represents 50% of this maximum value was used to set a threshold to define expression of ligands (from SCP) or receptors (from SKPs or blastemas). A curated ligand and receptor pair database (Qiao et al., 2014; S.A.Y. and F.D.M., unpublished data) was

used to identify ligands and receptors that were above the 50% expression threshold. The expression of a ligand (in SCPs) and the expression of a known cognate receptor (in SKPs or blastemas) was then used to predict potential paracrine interactions between SCPs and SKPs or SCPs and blastemas. Paracrine interaction predictions were visualized in Cytoscape (Version 3.1.0) where nodes (except for the SCPs, SKPs or Blastema nodes) represent ligands mediating potential paracrine interactions between the indicated populations and edges indicate the direction of interactions between the indicated populations.

Supplemental References

Arnold, K., Sarkar, A., Yram, M.A., Polo, J.M., Bronson, R., Sengupta, S., Seandel, M., Geijsen, N., and Hochedlinger, K. (2011). Sox2(+) adult stem and progenitor cells are important for tissue regeneration and survival of mice. Cell Stem Cell *9*, 317–329.

Bustin, S.A., Benes, V., Garson, J.A., Hellemans, J., Huggett, J., Kubista, M., Mueller, R., Nolan, T., Pfaffl, M.W., Shipley, G.L., et al. (2009). The MIQE guidelines: minimum information for publication of quantitative real-time PCR experiments. Clin. Chem. *55*, 611–622.

Carpenter, A.E., Jones, T.R., Lamprecht, M.R., Clarke, C., Kang, I.H., Friman, O., Guertin, D.A., Chang, J.H., Lindquist, R.A., Moffat, J., et al. (2006). CellProfiler: image analysis software for identifying and quantifying cell phenotypes. Genome Biol. *7*, R100.

Carvalho, B.S., and Irizarry, R.A. (2010). A framework for oligonucleotide microarray preprocessing. Bioinforma. *26*, 2363–2367.

Danielian, P.S., Muccino, D., Rowitch, D.H., Michael, S.K., and McMahon, A.P. (1998). Modification of gene activity in mouse embryos in utero by a tamoxifen-inducible form of Cre recombinase. Curr. Biol. *8*, 1323–1326.

Ellis, P., Fagan, B.M., Magness, S.T., Hutton, S., Taranova, O., Hayashi, S., McMahon, A., Rao, M., and Pevny, L. (2004). SOX2, a persistent marker for multipotential neural stem cells derived from embryonic stem cells, the embryo or the adult. Dev. Neurosci. *26*, 148–165.

Fernandes, K.J.L., McKenzie, I.A., Mill, P., Smith, K.M., Akhavan, M., Barnabé-Heider, F., Biernaskie, J., Junek, A., Kobayashi, N.R., Toma, J.G., et al. (2004). A dermal niche for multipotent adult skin-derived precursor cells. Nat. Cell Biol. *6*, 1082–1093.

Hamilton, T.G., Klinghoffer, R.A., Corrin, P.D., and Soriano, P. (2003). Evolutionary divergence of platelet-derived growth factor alpha receptor signaling mechanisms. Mol. Cell. Biol. *23*, 4013–4025.

Madisen, L., Zwingman, T.A., Sunkin, S.M., Oh, S.W., Zariwala, H.A., Gu, H., Ng, L.L., Palmiter, R.D., Hawrylycz, M.J., Jones, A.R., et al. (2010). A robust and high-throughput Cre reporting and characterization system for the whole mouse brain. Nat. Neurosci. *13*, 133–140.

Martin, D.C., Semple, J.L., and Sefton, M.V. (2010). Poly(methacrylic acid-co-methyl methacrylate) beads promote vascularization and wound repair in diabetic mice. J. Biomed. Mater. Res. A *93*, 484–492.

Ovchinnikov, D. (2009). Alcian blue/alizarin red staining of cartilage and bone in mouse. Cold Spring Harb. Protoc. *2009*, pdb.prot5170.

Shao, C., Liu, M., Wu, X., and Ding, F. (2007). Time-dependent expression of myostatin RNA transcript and protein in gastrocnemius muscle of mice after sciatic nerve resection. Microsurgery *27*, 487–493.

Simkin, J., Han, M., Yu, L., Yan, M., and Muneoka, K. (2013). The mouse digit tip: from wound healing to regeneration. Methods Mol. Biol. *037*, 419–435.

Taranova, O.V., Magness, S.T., Fagan, B.M., Wu, Y., Surzenko, N., Hutton, S.R., and Pevny, L.H. (2006). SOX2 is a dose-dependent regulator of retinal neural progenitor competence. Genes Dev. *20*, 1187–1202.

Wu, S., Wu, Y., and Capecchi, M.R. (2006). Motoneurons and oligodendrocytes are sequentially generated from neural stem cells but do not appear to share common lineage-restricted progenitors in vivo. Dev. *133*, 581–590.